*Research supported by the U. S. Atomic Energy Commission. The computer analysis has been made possible by a grant from the University of Rochester. This paper is an updated and final version of previous University of Rochester Reports No. 312 and No. 354.

†Presently at Monroe Community College, Rochester, New York.

‡A. P. Sloan Research Fellow.

[1]For a review of the status of the Q enhancement see: A. Firestone, in *Experimental Meson Spectroscopy – 1970,* edited by C. Baltay and A. H. Rosenfeld (Columbia Univ. Press, New York, 1970), p. 229; and also P. Slattery, University of Rochester Report No. UR-875-332, 1971 (unpublished).

[2]See the recent analysis of Q production in the reactions $K_L^0 p \to Q^0 p$ and $K_L^0 p \to \overline{Q}^0 p$ of G. Brandenburg *et al.* Nucl. Phys. B45, 397 (1972). The authors find that the cross section for nondiffractive Q production is approximately 30 μb near 7 GeV/c. This value is quite compatible with what we expect on the basis of the present calculation (see text).

[3]Application of the same procedure to the analogous data for the reaction: $\pi^- n \to \pi^- \rho^- p$ at 7 GeV/c, shown in Fig. 2 of D. Cohen *et al.*, Phys. Rev. Letters 28, 1601 (1972), yields $\gtrsim 100$ "A_1" events. This signal is consistent in size with the signal observed when the appropriate double-Regge cuts are applied to those data.

[4]The cross-hatched area in Fig. 2(d) corresponds to a cross section similar to that obtained for Q^0 in the fit shown in Fig. 2(a). In Fig. 2(f) we expect about 100 Q^{++} events on the basis of the model which we are about to discuss.

[5]M. Good and W. Walker, Phys. Rev. 120, 1857 (1960); R. Deck, Phys. Rev. Letters 13, 169 (1964); M. Ross and Y. Yam, *ibid.* 19, 546 (1967).

[6]E. Berger, Phys. Rev. 166, 1525 (1968).

[7]B. Werner *et al.*, Phys. Rev. 188, 2023 (1969); C. Y. Chien *et al.*, Phys. Letters 29B, 433 (1969); S. U. Chung *et al.*, Phys. Rev. 182, 1443 (1969).

[8]M. Farber *et al.*, Phys. Rev. Letters 22, 1394 (1969); J. Andrews *et al.*, *ibid.* 22, 738 (1969); H. Yuta, University of Rochester Report No. UR-875-271, 1969 (unpublished).

[9]A similar calculation performed by F. Bomse and R. Moses, Phys. Rev. 176, 2163 (1968), also predicts a low-mass $K^*\pi$ enhancement. Also see the analogous work pertaining to the A_1 in F. Winkelmann, R. Mickens, and H. J. Lubatti, Nucl. Phys. B30, 535 (1971), and in Ref. 3.

[10]The quantities $d\sigma/dt|_{\text{exp}}$ were calculated in the manner described in Ref. 3.

[11]These values of mass and width are similar to those which were found to describe the Q^+ signal produced in 12.7-GeV/c K^+p interactions, see M. Farber *et al.*, Phys. Rev. D 1, 78 (1970). We have widened the Γ_{CE} to account for the different widths observed in Fig. 4. When fitting mass spectra we use a distorted Breit-Wigner: The simple Breit-Wigner form is multiplied by the polynomial employed to describe the background.

[12]G. Fox, in *Experimental Meson Spectroscopy – 1972,* proceedings of the Third International Conference, Philadelphia, 1972, edited by Kwan-Wu Li and A. H. Rosenfeld (A.I.P., New York, 1972).

[13]E. Berger, in *Phenomenology in Particle Physics, 1971,* proceedings of the conference held at Caltech, 1971, edited by C. B. Chiu, G. C. Fox, and A. J. G. Hey (Caltech, Pasadena, 1971); P. H. Frampton and N. A. Törnqvist, CERN Report No. CERN-TH 1457; H. I. Miettinen, Proceedings of the Zakopane Colloquium, 1972 (unpublished).

PHYSICAL REVIEW D VOLUME 7, NUMBER 5 1 MARCH 1973

$\pi\pi$ Partial-Wave Analysis from Reactions $\pi^+p \to \pi^+\pi^-\Delta^{++}$ and $\pi^+p \to K^+K^-\Delta^{++}$ at 7.1 GeV/c†

S. D. Protopopescu,* M. Alston-Garnjost, A. Barbaro-Galtieri, S. M. Flatté,‡ J. H. Friedman,§ T. A. Lasinski, G. R. Lynch, M. S. Rabin,‖ and F. T. Solmitz
Lawrence Berkeley Laboratory, University of California, Berkeley, California 94720

(Received 25 September 1972)

We present results of an energy-dependent phase-shift analysis for $\pi\pi$ energies between 550 and 1150 MeV from reactions $\pi^+p \to \pi^+\pi^-\Delta^{++}$ and $\pi^+p \to K^+K^-\Delta^{++}$ at 7.1 GeV/c. The $I=0$ s wave is parametrized in terms of a 2×2 M-matrix coupling $\pi\pi$ and $K\overline{K}$ channels. All the obtained solutions rule out the possibility of a narrow ϵ resonance in the ρ region and are characterized by a very rapid variation of the $I=0$ s-wave amplitude near $K\overline{K}$ threshold. We show that this rapid variation can be explained by a pole in the second Riemann sheet close to the $K\overline{K}$ threshold.

I. INTRODUCTION

Because of its theoretical simplicity, the s-wave $\pi\pi$ scattering amplitude has been the subject of substantial experimental and theoretical work over many years.[1] The experimental work has depended on the use of reactions dominated by pion exchange; the analysis of these reactions has yielded some information in the region of the ρ meson, but a persistent ambiguity in the s-wave amplitude between 750 and 900 MeV has made any conclusions drawn from the data very uncertain.

Recently, in the reaction $\pi^+p \to \pi^+\pi^-\Delta^{++}$, we have observed a strong anomaly in the $\pi\pi$ system near $K\overline{K}$ threshold[2]; this anomaly consists of a shoulder followed by a rapid drop in the cross section be-

tween 950 and 980 MeV, and a striking discontinuity in the Y_1^0 moment at 980 MeV. The data agree nicely with the interpretation that this anomaly arises from unitarity and a strong coupling of the s-wave $\pi\pi$ channel to the $K\bar{K}$ channel at threshold.[3] Furthermore, this interpretation provides a complete resolution of the ambiguity that has plagued the determination of the s-wave amplitude for many years.[3]

The important qualitative conclusions drawn from our data were reached without the need of a complicated analysis. In our previous paper no extrapolation to the pion pole was undertaken, and a simple Breit-Wigner form for the s wave near $K\bar{K}$ threshold (the S^* resonance) was used to show qualitatively how the effect might be interpreted. However, a more quantitative analysis is desirable: That is the subject of this paper. We have added extrapolation to the pole, $I=2$ waves, inelasticity in the p and d waves, an f wave, and a two-channel M-matrix treatment of the s-wave amplitude.

Most of the information on $\pi\pi$ phase shifts so far has come from reactions of the form $\pi N \to \pi\pi N$.[1] Extrapolations to the π pole, using this reaction, suffer from the fact that the amplitudes contain a kinematical zero somewhere between $t_{NN}=\mu^2$ (π mass squared) and $t_{NN}=0$. Because of absorption effects the position of this zero is not known with precision and may occur at different values of t_{NN} for each partial-wave amplitude. This makes results of extrapolations uncertain. Reactions of the form $\pi N \to \pi\pi\Delta$ do not have this problem; therefore, one can extrapolate the normalized Y_L^0 moments. In addition, one can check the validity of the extrapolation by comparing the extrapolated Y_L^0 moments of the $\pi^+ p$ vertex with the moments for physical $\pi^+ p$ scattering. These advantages are partially offset by the fact that $|t_{N\Delta\,\min}|$ (minimum momentum transferred squared) is larger, requiring an extrapolation over a larger interval of $t_{N\Delta}$. Because of these problems a detailed analysis from a single experiment cannot be expected to give definitive values for the phases and inelasticities. In the absence of physical $\pi\pi$ scattering one can only hope that a consistent set of solutions may emerge from various different reactions at different energies.

We present here results of a $\pi\pi$ phase-shift analysis by using the reactions

(1) $\pi^+ p \to \pi^+\pi^-\Delta^{++}$ (32 100 events, $|t_{p\Delta}|<0.4$ GeV^2),

(2) $\pi^+ p \to K^+K^-\Delta^{++}$ (682 events, $|t'_{p\Delta}|=|t-t_{\min}|<0.1$ GeV^2),

at an incident beam momentum of 7.1 GeV/c. Data from reaction $\pi^+ p \to K^0\bar{K}^0\Delta^{++}$ are also used to estimate non-π-exchange background contribution to reaction (2). In addition, we present data from 4π systems recoiling against the Δ^{++} which are relevant for estimating inelasticities but will not be used explicitly in the analysis.

In Sec. II we discuss the experimental data. In Sec. III we discuss how the extrapolation to the π pole is done. To obtain the $\pi^+\pi^- \to \pi^+\pi^-$ cross section we perform a linear Chew-Low extrapolation in $t_{p\Delta}$ modified by Dürr-Pilkuhn form factors. The Y_L^0 moments are obtained by a simple linear extrapolation in $t_{p\Delta}$. In Sec. IV we present a parametrization of the partial-wave amplitudes which we use to fit the extrapolated cross section and Y_L^0 moments (up to $L=6$) between 550 and 1150 MeV. The I (isospin) = 2 amplitudes are assumed to be elastic everywhere, the $L\neq 0$ ($I\neq 2$) amplitudes are allowed to become inelastic at the $\omega\pi$ threshold (~900 MeV). The $I=0$ s wave is described by a 2×2 M matrix which couples $\pi\pi$ and $K\bar{K}$ channels. The results of the fits are given in Sec. V. They agree with the results of our previous analysis in that our δ_0^0 rules out the "up" solution (narrow ϵ) in the 800- to 900-MeV region and varies rapidly before the $K\bar{K}$ threshold ($\delta_0^0=90°$ at ~900 MeV, $\delta_0^0=180°$ at ~990 MeV). All the fits with reasonable χ^2 gave essentially the same phases and inelasticities within the computed errors. Using our M-matrix parameters, we looked for poles in the $I=0$ s-wave amplitude. We always found one pole (S^*) on the second Riemann sheet at $997\pm 6 - i(27\pm 8)$, which can be interpreted as a $K\bar{K}$ bound state. We also found another pole (ϵ) on the second Riemann sheet at $660\pm 100 - i(320\pm 70)$, but when we fitted with slightly different parametrizations we obtained fits with similar phase shifts which did not have an ϵ pole in the second Riemann sheet. This indicates that considerably more data (especially below 550 MeV) are needed to be able to locate faraway poles. Also, the effect of the 4π cut (which we neglect) might have to be included.

In Sec. VI we do an energy-independent phase-shift analysis between 500 and 930 MeV, assuming that only elastic s and p waves are present. We show that between 700 and 880 MeV one cannot eliminate the usual "up-down" ambiguity on a point-by-point basis using the Y_1^0 and Y_2^0 moments alone, but near 900 MeV the "down" solution ($\delta_0^0\approx 90°$) seems to be strongly favored. In Sec. VII we present data for the three-body systems ($\pi^+\pi^+\pi^-$ and $\pi^-\pi^+ p$) to show that three-body resonances do not seem to contribute significant background. We also show how model-dependent absorption corrections may modify our results and discuss the effect of ρ-ω interference on the extrapolation. We summarize our results in Sec. VIII. In Appendix A we

discuss in more detail the possibility of additional poles in the S^* region. In Appendix B we give tables of the extrapolated cross sections and moments used in the analysis.

II. DATA REDUCTION

A. Path Length

We used two methods to compute the path length: (1) count the number of beam tracks and (2) count the total number of events and divide by the total cross section (σ_{tot}).

With the first method we obtained 44.8 ± 0.4 events/μb. For the second we used $\sigma_{tot} = 25.5 \pm 0.3$ mb given by Dardel *et al.*,[4] and obtained 42.8 ± 1.2 events/μb. The largest uncertainty in the second method is in estimating the loss of forward elastic events because of short proton tracks. Using the t_{pp} distribution of elastic $\pi^+ p$ events obtained by Foley *et al.*,[5] we estimated that we lose about 38% of the elastic events. The lower value obtained with this method as compared to the first reflects the amount of μ^+ contamination in our beam (between 2% and 3%). Therefore, the second value was used for computing cross sections. More details on the path length computation are given in Ref. 6.

B. Scanning and Measuring

About 20% of the film was scanned twice and 10% was scanned three times. The total number of events found was 1 025 200 of which 415 600 were 2-prong events, 421 650 4-prong events, and 107 170 6-prong events. The rest are higher prong events and other topologies. We used the simple Geiger-Werner method for calculating scanning efficiencies, which should be quite adequate for 4-, 6-, and 2-prong events (excepting those with short proton tracks) since no subsamples are expected to be harder to see than others. The third scan was used to check the calculated scanning efficiencies; we found the values to be consistent within the quoted errors. The scanning efficiencies are given in Table I. The events were measured on the spiral reader.

For data reduction the LBL Group A programs POOH, TVGP, and SQUAW were used. Failing events were measured a second time (excepting 2-prong events). The over-all measuring efficiency for 4- and 6-prong events is $95 \pm 1.0\%$. The particular sample of 4C (4-constraint) 4-prong events used in the analysis had further selections made in the fitting programs, which resulted in an effective measuring efficiencies of $90 \pm 1.5\%$. Details on the determination of scanning and measuring efficiencies are given in Ref. 7.

C. Selection of Data Used in the Analysis

The following reactions will be of indirect or direct interest:

(1) $\pi^+ p \to \pi^+\pi^-\pi^+ p$, 72 700 events,
(2) $\pi^+ p \to K^+K^-\pi^+ p$, 4600 events,
(3) $\pi^+ p \to \pi^+\pi^-\pi^+\pi^-\pi^+ p$, 15 460 events,
(4) $\pi^+ p \to \pi^+\pi^-\pi^+ p$MM (missing mass $\geq 2\pi^0$), 113 570 events,
(5) $\pi^+ p \to \pi^+ p\bar{K}^0(K^0)$ (One K^0 decays to $\pi^+\pi^-$, the other is not seen.), 1270 events,
(6) $\pi^+ p \to \pi^+ p K^0\bar{K}^0$ (Both K^0's are seen to decay to $\pi^+\pi^-$ in bubble chamber.), 286 events.

We will only study the systems recoiling against a Δ^{++}; we define the Δ^{++} as the $\pi^+ p$ combination with mass in the interval 1.13 to 1.36 GeV. Where more than one $\pi^+ p$ combination lies in that interval the combination with the smallest $|t_{p\Delta}|$ is chosen as the Δ^{++}. The number of events with more than one Δ^{++} candidate is considerably reduced with a small t cut. Of the 32 100 $\pi^+\pi^-\Delta^{++}$ events with $|t_{p\Delta}| < 0.4$ GeV^2 (which we will study in great detail), only 5% are ambiguous. From the mass and t distribution for ambiguous events we estimate that no more than 300 events may be misinterpreted (or may be double Δ^{++} events) by our selection criteria. About 15% of the $K^+K^-\pi^+ p$ (2) events are ambiguous with $\pi^+\pi^-\pi^+ p$ (1) events. After we select events with a Δ^{++} and $|t'_{p\Delta}| \equiv |t_{p\Delta} - t_{\min}| \leq 0.1$ GeV^2, only 17 out of 682 events are ambiguous (2.5%). The $\pi^+ p\bar{K}^0(K^0)$ (5) events have a high percentage of ambiguities, and we shall discuss a

TABLE I. Scanning and measuring efficiencies.

Event type	No. of events	Scanning efficiency (%)	Measuring efficiency (%)
2-prong	415 600	93.9± 0.5	(Note *a*)
4-prong	421 650	98± 1	95± 1
6-prong	107 170	96.8± 0.5	95± 1
Others[a]	70 200	95± 2	...
$\pi^+\pi^-\Delta^{++}$ [b]	32 000	98± 1	90± 1
$K^+K^-\Delta^{++}$ [c]	682	98± 1	90± 1

[a] Measuring efficiency has not been determined yet for these events.
[b] These are the events used for extrapolation to the π pole ($t_{p\Delta} < 0.4$ GeV^2).
[c] These are events used for computing the $\pi^+\pi^- \to K\bar{K}$ cross section.

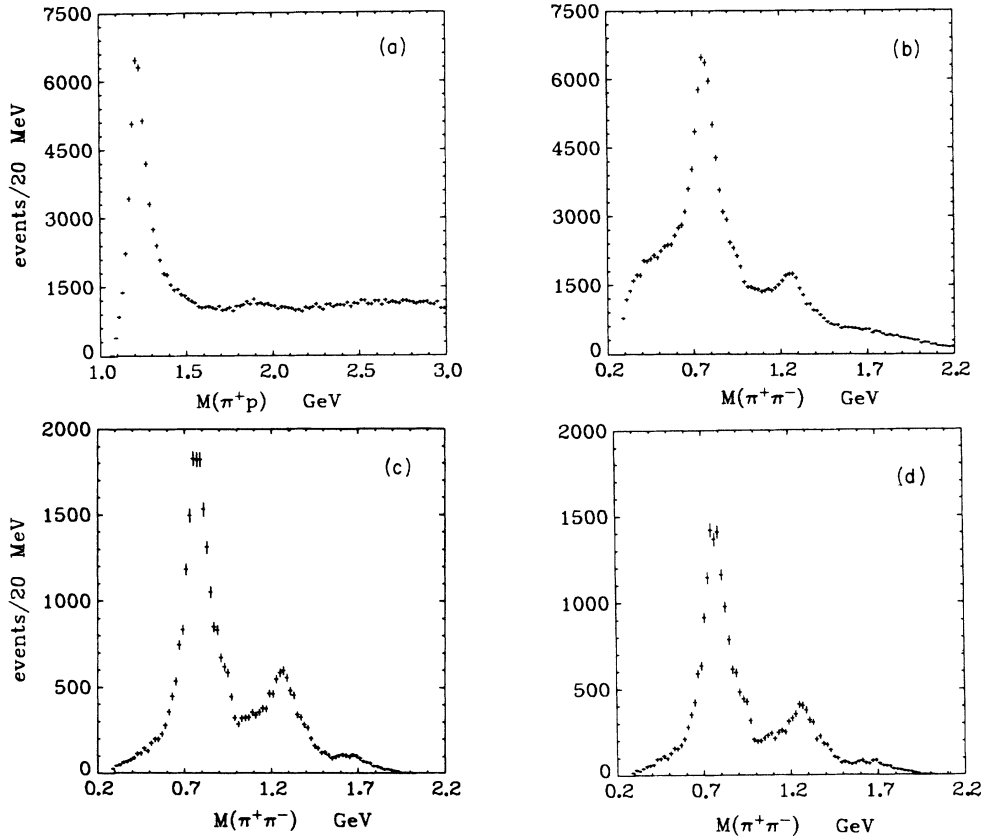

FIG. 1. Mass distributions for $\pi^+\pi^-\pi^+p$ events (reaction 1) in 20-MeV bins. (a) π^+p mass distribution, all events double counted; (b) $\pi^+\pi^-$ mass distribution, all events double counted; (c) $\pi^+\pi^-$ mass distribution with Δ^{++} selected and $|t_{p\Delta}|<0.4$ GeV^2; (d) same as (c) but $|t'_{p\Delta}|<0.1$ GeV^2.

restricted sample of them later on (Sec. III C). After the Δ^{++} selection we are left with the following:

(1′) $\pi^+p\to\pi^+\pi^-\Delta^{++}$, 32 100 events, $|t_{p\Delta}|<0.4$ GeV^2, 23 400 events, $|t'_{p\Delta}|<0.1$ GeV^2,
(2′) $\pi^+p\to K^+K^-\Delta^{++}$, 682 events, $|t'_{p\Delta}|<0.1$ GeV^2,
(3′) $\pi^+p\to\pi^+\pi^-\pi^+\pi^-\Delta^{++}$, 2470 events, $|t'_{p\Delta}|<0.1$ GeV^2,
(4′) $\pi^+p\to\pi^+\pi^-\mathrm{MM}\Delta^{++}$, 9600 events, $|t'_{p\Delta}|<0.1$ GeV^2,
(5′) $\pi^+p\to\bar{K}^0(K^0)\Delta^{++}$, 140 events, $|t'_{p\Delta}|<0.1$ GeV^2,
(6′) $\pi^+p\to\bar{K}^0K^0\Delta^{++}$, 63 events, $|t'_{p\Delta}|<0.1$ GeV^2.

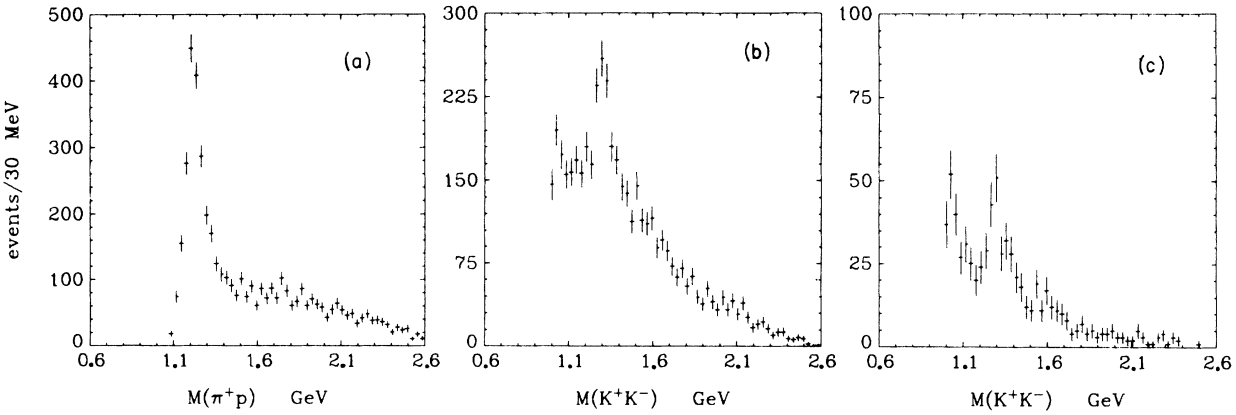

FIG. 2. Mass distribution for $K^+K^-\pi^+p$ events (reaction 2) in 30-MeV bins. (a) π^+p mass distribution, all events; (b) K^+K^- mass distribution, all events; (c) K^+K^- mass distribution with Δ^{++} selected and $|t'_{p\Delta}|<0.1$ GeV^2.

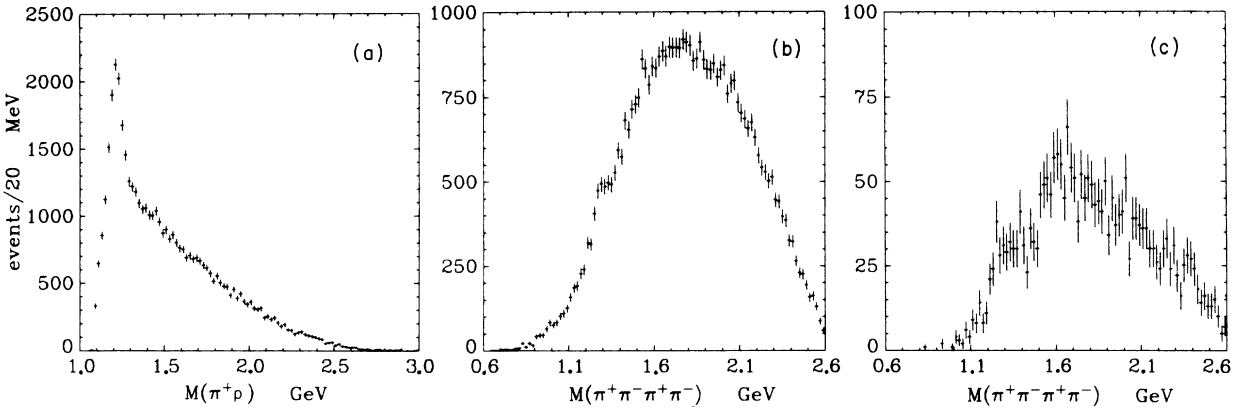

FIG. 3. Mass distribution for $\pi^+\pi^-\pi^+\pi^-\pi^+p$ events (reaction 3) in 20-MeV bins. (a) π^+p mass distribution, all events triple counted; (b) $\pi^+\pi^-\pi^+\pi^-$ mass distribution, all events triple counted; (c) $\pi^+\pi^-\pi^+\pi^-$ mass distribution with Δ^{++} selected and $|t'_{p\Delta}|<0.1$ GeV^2.

Part of these data have already been published in Ref. 2.

The mass distributions of the π^+p system and the systems recoiling against the Δ^{++} are shown in Figs. 1–6, both before and after the selections. For extrapolations to π pole of the $\pi^+\pi^-$ system we use events with $|t_{p\Delta}|<0.4$ GeV^2. The mass resolution of $\pi^+\pi^-$ events varies somewhat as a function of mass, being ±5 MeV in the ρ region (~760 MeV) and ±8 MeV in the f_0 region; the dependence on $\pi\pi$ angles is generally small. (For further details on mass resolution see Ref. 8.) Because we only consider events with small momentum transfer there are no ambiguities between π^+ and p tracks.

III. EXTRAPOLATION TO π POLE

If π exchange is dominant, the amplitude for the reaction $\pi^+p\to\pi^+\pi^-\Delta^{++}$ is of the form (ignoring effects of absorption)

$$A(s,t)\propto\frac{\langle\pi^+p|T|\pi^+p\rangle\langle\pi^+\pi^-|T|\pi^+\pi^-\rangle}{t-\mu^2}+X\,, \quad (3.1)$$

where X stands for processes not produced by π exchange, e.g., A_2 exchange, $\pi^+p\to A_2^+p$, $\pi^+p\to\pi^+N^{*+}$, etc. When $t\to\mu^2$, the first term diverges while X remains finite. The hope then is that by extrapolating to $t=\mu^2$ one removes off-shell effects and non-π-exchange contributions. After extrapolating, the analysis becomes simpler in the sense that a standard phase-shift analysis may be attempted. This simplicity is offset by the uncertainties in extrapolation procedures and the large increase in the statistical errors because of the need to divide the data in cells of t and $m_{\pi\pi}$. The uncertainty becomes larger the higher the mass because $|t_{\min}|$ increases ($t_{\min}=-1.3\mu^2$ at 760 MeV, $t_{\min}=-5.2\mu^2$ at 1280 MeV).

A. Evaluation of the $\pi^+\pi^-\to\pi^+\pi^-$ Cross Section

In the case of one-pion exchange (OPE), the differential cross section for the process $\pi^+p\to(\pi^+\pi^-)(\pi^+p)$ is given by (if we neglect background terms in Sec. III A)

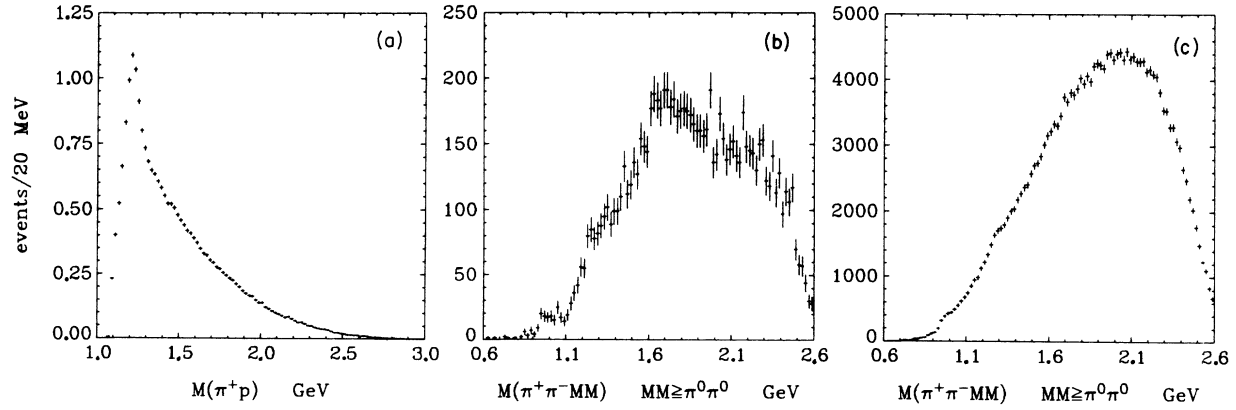

FIG. 4. Mass distribution for $\pi^+p\pi^+\pi^-$MM (missing mass $\geq 2\pi^0$) (reaction 4) in 20-MeV bins. (a) π^+p mass distribution, all events double counted; (b) $\pi^+\pi^-$MM mass distribution, Δ^{++} selected and $|t'_{p\Delta}|<0.1$ GeV^2; (c) $\pi^+\pi^-$MM mass distribution, all events double counted.

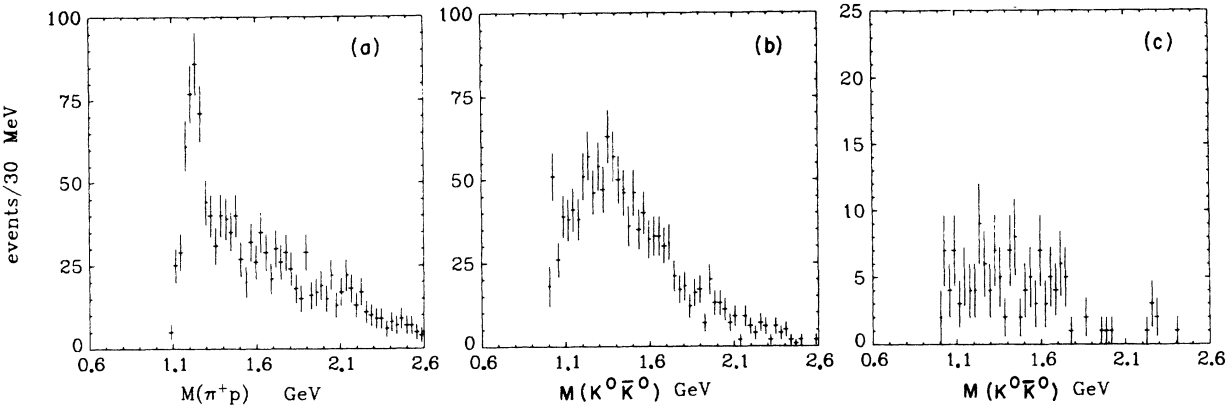

FIG. 5. Mass distribution for $\pi^+pK^0(\bar{K}^0)$ (reaction 5) in 30-MeV bins. (a) π^+p mass distribution, all events; (b) $K^0(\bar{K}^0)$ mass distribution, all events; (c) $K^0(\bar{K}^0)$ mass distribution with Δ^{++} selection and $|t'_{p\Delta}|<0.1$ GeV^2.

$$\frac{d^3\sigma}{dtdMdm}=\frac{1}{4\pi^3P_1^2E^2}(m^2q_t\sigma_{\pi\pi})\frac{G^2(t)}{(t-\mu^2)^2}(M^2Q_t\sigma_{\pi p}), \tag{3.2}$$

where

P_I = c.m. momentum, $m=\pi^+\pi^-$ invariant mass,
E = c.m. energy, $M=\pi^+p$ invariant mass,
$G(t)$ = form factor = 1 at π pole,
$\sigma_{\pi\pi}=\pi^+\pi^-$ cross section,
$\mu=\pi$ mass, $\sigma_{\pi p}=\pi^+p$ cross section,
q_t = virtual π momentum in $\pi^+\pi^-$ rest frame,
Q_t = virtual π momentum in π^+p^- rest frame.

In addition we define for later use

q = outgoing π^+ momentum in $\pi^+\pi^-$ rest frame,
Q = outgoing p momentum in π^+p rest frame.

We have then

$$q=\left(\frac{m^2}{4}-\mu^2\right)^{1/2},$$

$$Q=\frac{1}{2M}\{[M^2-(m_p+\mu)^2][M^2-(m_p-\mu)^2]\}^{1/2},$$

$$q_t=\left(\frac{(m^2+\mu^2-t)^2}{4m^2}-\mu^2\right)^{1/2},$$

$$Q_t=\left(\frac{(M^2+m_p^2-t)^2}{4M^2}-m_p^2\right).$$

The standard method of extrapolating is to calculate first

$$\sigma_{\rm OPE}\equiv\frac{1}{4\pi^3P_I^2E^2}\int_{m_1}^{m_2}dm\int_{t_1}^{t_2}dt\int_{M_1}^{M_2}dM\,m^2q_t\frac{G^2(t)}{(t-\mu^2)^2}M^2Q_t\sigma_{\pi p}. \tag{3.3}$$

The above is the integral of Eq. (3.2), where we have set $\sigma_{\pi\pi}=1$ mb and $\sigma_{\pi p}$ is the physical $\pi^+p\to\pi^+p$ scattering cross section. Then one fits to a polynomial in t the function[9]

$$F(m,t)=\left(\int_{m_1}^{m_2}dm'\int_{t_1}^{t_2}dt'\int_{M_1}^{M_2}dM\frac{d^3\sigma}{dt'dMdm'}\right)\Big/\sigma_{\rm OPE}, \tag{3.4}$$

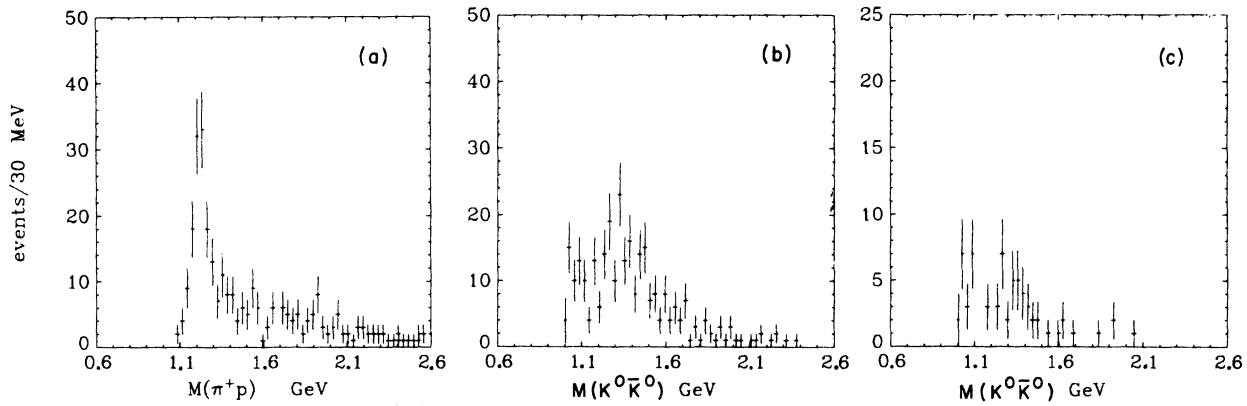

FIG. 6. Mass distribution for $\pi^+pK^0\bar{K}^0$ events (reaction 6) in 30-MeV bins. (a) π^+p mass distribution, all events; (b) $K^0\bar{K}^0$ mass distribution, all events; (c) $K^0\bar{K}^0$ mass distribution with Δ^{++} selected and $|t'_{p\Delta}|<0.1$ GeV^2.

where $m = \frac{1}{2}(m_1 + m_2)$ and $t = \frac{1}{2}(t_1 + t_2)$. The cross section for $\pi^+\pi^-$ is then given by $\sigma_{\pi\pi}(m) = F(m, t=\mu^2)$.

With this procedure one usually needs high-order polynomials in t to obtain good results. A linear, or at most quadratic, extrapolation seems to be quite adequate for our data if we modify σ_{OPE} with Dürr-Pilkuhn (DP) form factors. The disadvantage is that one must know in advance the amounts of each wave present [see Eq. (3.5) below]. Fortunately, the effect of DP form factors is not very drastic, so a rough estimate is quite adequate.

The DP method consists in replacing[10]

$$q_t \to q \quad \text{for } s \text{ wave},$$

$$q_t \to \left(\frac{q_t}{q}\right)^2 \left(\frac{1+R_\rho{}^2 q^2}{1+R_\rho{}^2 q_t{}^2}\right) q \quad \text{for } p \text{ wave}, \tag{3.5}$$

$$q_t \to \left(\frac{q_t}{q}\right)^4 \left(\frac{9+3R_d{}^2 q^2 + R_d{}^4 q^4}{9+3R_d{}^2 q_t{}^2 + R_d{}^4 q_t{}^4}\right) q \quad \text{for } d \text{ wave}.$$

For the Δ^{++} vertex the modification is slightly different:

$$Q_t \to \frac{(M+m_\rho)^2 - t}{(M+m_\rho)^2 - \mu^2}\left(\frac{Q_t}{Q}\right)\frac{1+R_\Delta{}^2 Q^2}{1+R_\Delta{}^2 Q_t{}^2} Q\,. \tag{3.6}$$

Using these form factors, Wolf[11] could fit very well the t distributions in the ρ region (for $\pi^+ p \to \pi^+\pi^-\Delta^{++}$) at various beam energies with $R_\rho = 8.28 \pm 0.2$ GeV^{-1} and $R_\Delta = 3.97 \pm 0.11$ GeV^{-1}. In addition he had to introduce a slowly varying function:

$$G(t) = \frac{c-\mu^2}{c+t}, \quad \text{where} \quad c = 2.29 \pm 0.27 \text{ GeV}^2\,.$$

These values have also given satisfactory fits to other reactions.[12] We made least-squares fits to t distributions for different $\pi\pi$ mass regions, assuming that the p and d waves are given by ρ and f_0 mesons, and that the s wave is smooth and of the order of 13% of the cross section. We found that R_ρ and R_Δ are strongly correlated. If R_Δ is kept fixed at 4.0 GeV^{-1}, then the best value for R_ρ was found to be 8.2 GeV^{-1}, in good agreement with Wolf's value. In Fig. 7 we show the result of a fit to the t distribution for $0.76 < M_{\pi\pi} < 0.78$ GeV. A least-squares fit to the f_0 region, keeping R_ρ and R_Δ fixed, showed that the value of R_d tends to be large and the fit is not very sensitive to it as long as $R_d \geq 14.0$ GeV^{-1}.

For calculating σ_{OPE} we used $R_\Delta = 4.0$ GeV^{-1}, $R_\rho = 8.2$ GeV^{-1}, $R_d = 14.0$ GeV^{-1}, and took $\sigma_{\pi^+ p}$ from Carter *et al.*[13] We then did a least-squares fit to

$$F(m,t) = a + bt \quad (\text{note that } \sigma_{\pi\pi} = a + b\mu^2) \tag{3.7}$$

to determine a and b for various mass bins. Mass bins were chosen of variable width so as to have roughly the same number of events in each bin. In the range 0.6 to 1.4 GeV the χ^2 for a linear fit was good, varying between 3.0 and 6.0 for 5 degrees of freedom. A quadratic fit did not improve χ^2 significantly in that energy range, and the extrapolated values were compatible with the ones obtained by a linear extrapolation, but the errors on the extrapolated points were substantially larger. Below 600 MeV, linear fits had poor χ^2 (≥ 10.0); quadratic fits were found to be much better.

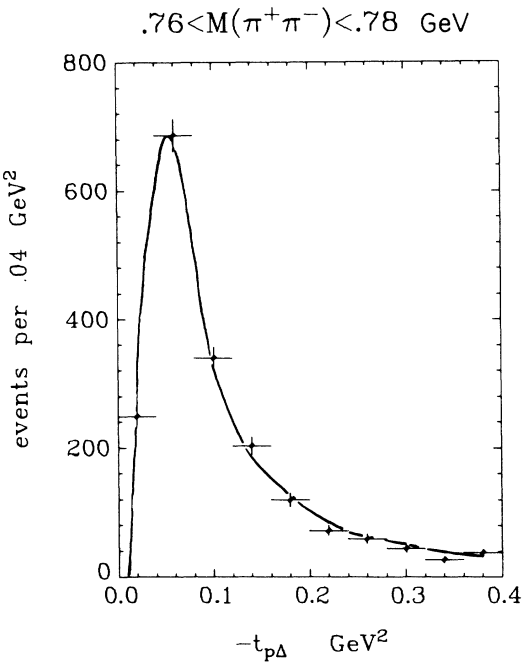

FIG. 7. $-t_{p\Delta}$ distribution for $0.76 < m_{\pi\pi} < 0.78$ GeV, for reaction $\pi^+ p \to \pi^+\pi^-\Delta^{++}$. Curve corresponds to a fit with Dürr-Pilkuhn form factors.

Extrapolations were tried for many different t intervals and also using the x variable of Baton *et al.*[14] Results varied little. The cross section shown in Fig. 8 was obtained with a linear extrapolation in t ($|t| < 0.4$ GeV^2) for points above 600 MeV. Below 600 MeV the extrapolation was quadratic in t. We obtained, at 760 MeV, $\sigma_{\pi\pi} = 133.4 \pm 4.8$ mb; and at 1280 MeV, $\sigma_{\pi\pi} = 31.2 \pm 2.0$ mb. The quoted errors are statistical. The unitary limits at those masses are

$I = 1$, p wave, 116 mb at 760 MeV ($12\pi\lambda^2$),
$I = 0$, s wave, 17 mb at 760 MeV ($\frac{16}{9}\pi\lambda^2$),
$I = 0$, d wave, 27.9 mb at 1280 MeV ($\frac{80}{9}\pi\lambda^2$),
$I = 0$, s wave, 5.6 mb at 1280 MeV ($\frac{16}{9}\pi\lambda^2$).

B. Extrapolation of Y_L^0 Moments

To extrapolate the moments we simply calculate

$$\langle Y_L^0 \rangle(m,t) = \left(\sum_{i=1}^{N} Y_{L,i}^0\right)\Big/ N\,, \tag{3.8}$$

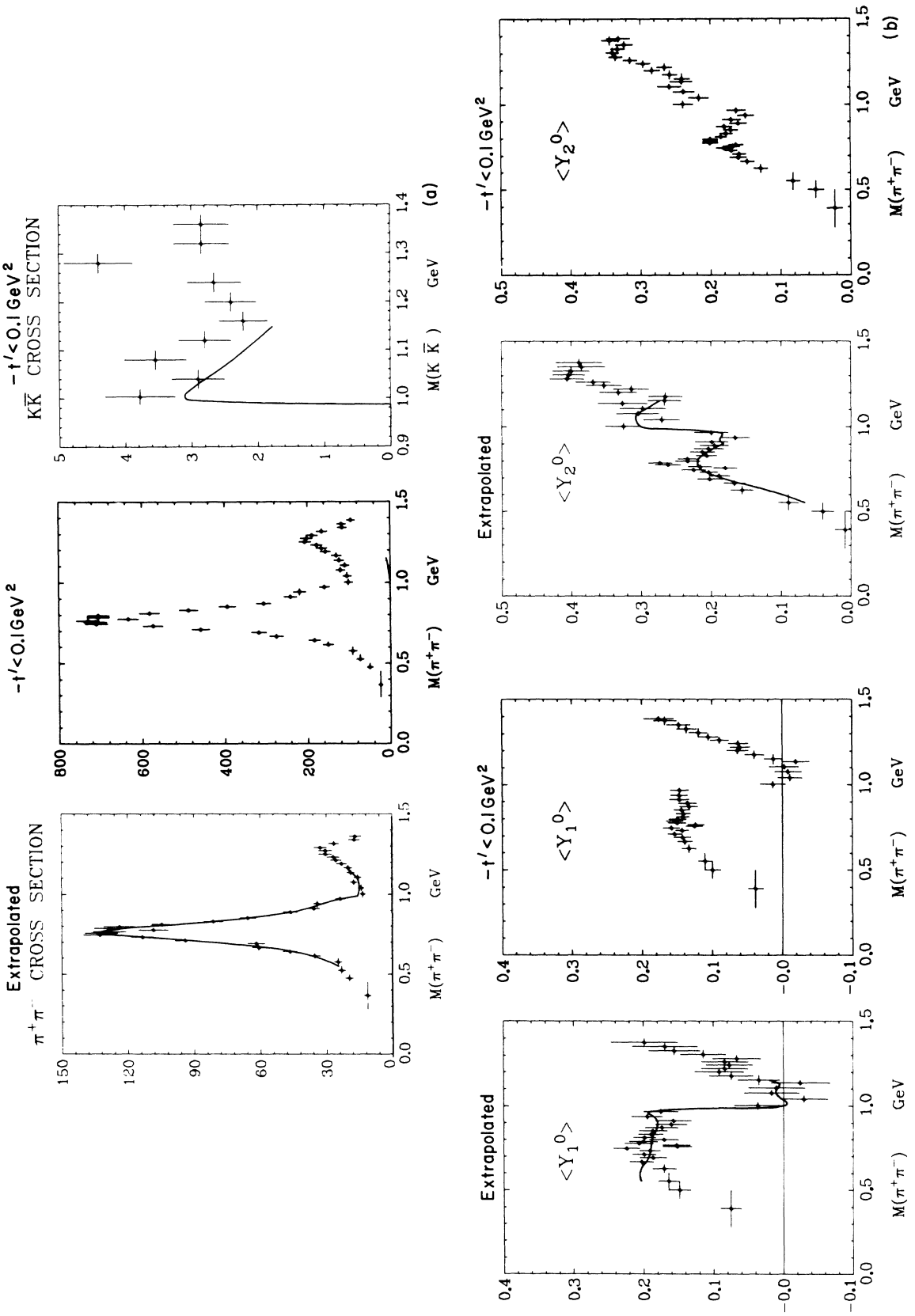

FIG. 8. *(Continued on following page.)*

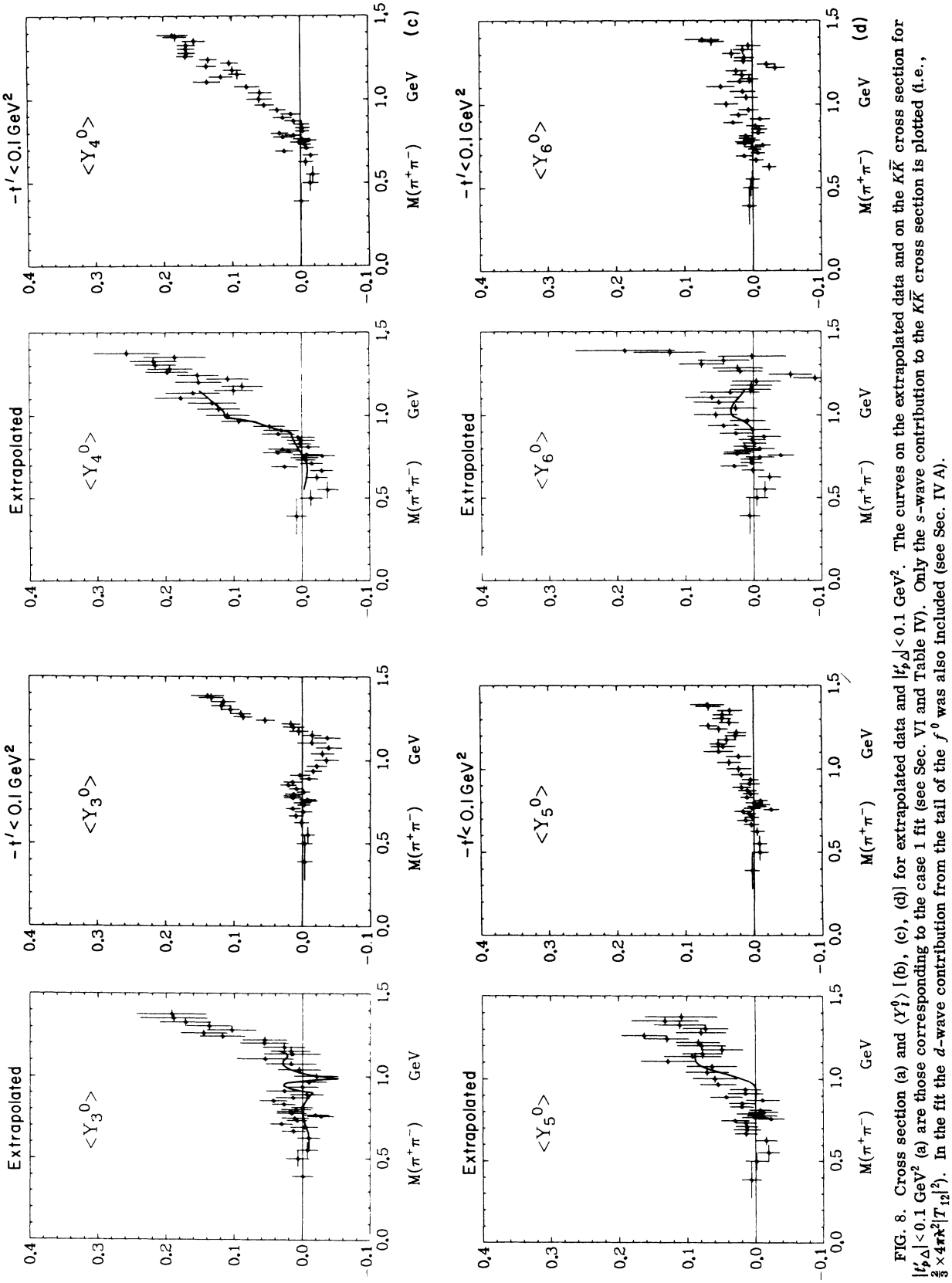

FIG. 8. Cross section (a) and $\langle Y_l^0 \rangle$ [(b), (c), (d)] for extrapolated data and $|t'_p\Delta|<0.1$ GeV^2. The curves on the extrapolated data and on the $K\bar{K}$ cross section for $|t'_p\Delta|<0.1$ GeV^2 (a) are those corresponding to the case 1 fit (see Sec. VI and Table IV). Only the s-wave contribution to the $K\bar{K}$ cross section is plotted (i.e., $\frac{2}{3}\times 4\pi\lambda^2|T_{12}|^2$). In the fit the d-wave contribution from the tail of the f^0 was also included (see Sec. IV A).

where N is the number of events in (m, t) cell, and fit $\langle Y_L^0\rangle(m, t)$ for each m to a function $a+bt$. The $\pi\pi$ $\langle Y_L^0\rangle$ is assumed to be equal to $\langle Y_L^0\rangle(m, \mu^2)$. Various intervals in t were tried, and the results were always consistent with each other. The ones shown on Figs. 8(b)–8(d) were calculated for $|t| \leq 0.4$ GeV^2. Quadratic extrapolations only increased errors substantially without improving χ^2 significantly. Extrapolations using the variable x of Baton *et al.*[14] were found to be unsatisfactory, often giving values that were too high and would violate unitarity for some of the partial waves.

Since the moments are normalized we can neglect kinematic factors. In principle, no factors would be needed if off-shell effects were the same for each partial wave. We find that by including DP form factors we can change the results by at most 1%, while the errors on extrapolated points are usually of the order of 10%. Unknown phases in the form factors may introduce larger corrections, but we know of no reliable way to estimate how important these phases may be.

The validity of the extrapolation procedure can be checked by looking at Y_L^0 for the π^+p vertex as a function of π^+p and $\pi\pi$ mass. They should show no dependence on $\pi^+\pi^-$ mass. Linear extrapolations of Y_1^0 show striking agreement with the values for π^+p elastic scattering (Fig. 9), except for $\pi\pi$ mass below 600 MeV, which makes the region suspect. We have no adequate explanation as to why the extrapolation should fail at low $\pi\pi$ mass. It is worth emphasizing that if the Δ^{++} was produced by some process other than π exchange, there is no reason to expect Y_1^0 to behave as observed in physical π^+p scattering, since that moment is determined by the interference between S and P waves; a pure Δ state would give $Y_1^0 = 0$. The extrapolated Y_2^0 moment (Fig. 10) also agrees quite well with the one observed in physical π^+p scattering, but this is a weaker check, since any reaction where the P_{33}, $M = \frac{3}{2}$ wave dominates will give a similar Y_2^0 moment. These results give us more confidence in the validity of the extrapolation but they do not constitute a proof.

C. Determination of $\pi^+\pi^- \to K\bar{K}$ Cross Section

Since we do not have enough K^+K^- events to perform a meaningful extrapolation, we chose to calculate the $K\bar{K}$ cross section by comparing the number of $K^+K^-\Delta^{++}$ events to $\pi^+\pi^-\Delta^{++}$ events for $|t'_{p\Delta}| < 0.1$ GeV^2. Note that K^+K^- may consist of a mixture of $C=+1$ and $C=-1$ states. Only $C=+1$ can come from π exchange. We use the meager information available from $K^0\bar{K}^0$ Δ^{++} events to

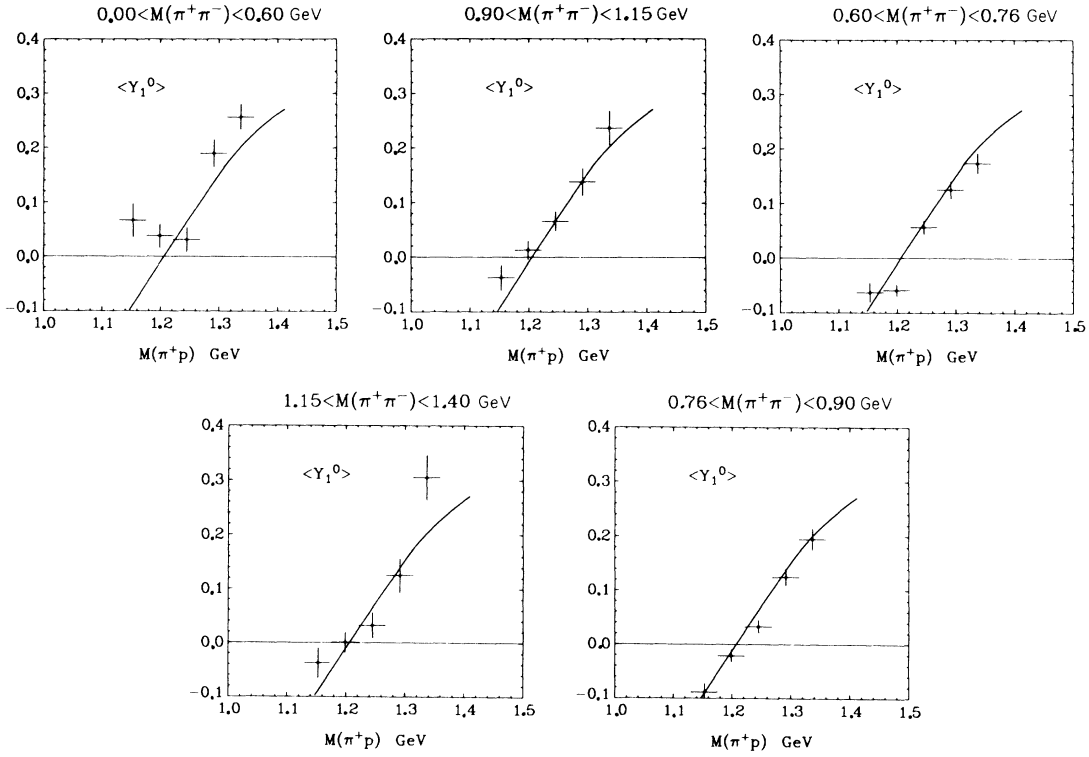

FIG. 9. Extrapolated $\langle Y_1^0\rangle$ moments for π^+p vertex. Curves correspond to physical π^+p scattering.

estimate the relative amounts of $C=+1$ and $C=-1$ events. For $K\bar{K}$ mass less than 1.1 GeV and $t'_{p\Delta}$ <0.1 GeV^2, we have

(1) $\pi^+p \to K^+K^-\Delta^{++}$, 146 events,
(2) $\pi^+p \to \bar{K}^0(K^0)\Delta^{++}$ [only one K^0 decaying in the bubble chamber (to $\pi^+\pi^-$)], 19 events,
(3) $\pi^+p \to \bar{K}^0K^0\Delta^{++}$ [both K^0's decaying in the bubble chamber], 18 events.

All of the events in reaction (3) must be K_SK_S which have $C=+1$, and some percentage of reaction (2) may be K_SK_L with $C=-1$. Of the 19 events with one K^0 decay not seen (2), eight are ambiguous with $\pi^+K^+K^0$MM (missing mass $\geq \pi^0n$) although for four of them bubble density favors strongly the $K^0\bar{K}^0\,\pi^+p$ interpretation. We expect 5% of K_S to decay outside the bubble chamber and another 5% to decay too close to the vertex to be identified as a vee. These effects add up to a 20% correction for reaction (3). In addition, there is another 10% correction because scanning and measuring efficiencies are lower for reactions (2) and (3) than for reaction (1). Since a K_S decays $\frac{2}{3}$ of the time into $\pi^+\pi^-$, we expect $\frac{4}{9}$ of the K_SK_S events to contribute to reaction (2) and another $\frac{4}{9}$ to reaction (3). Since the number of events in both reactions is equal within statistics, they are clearly consistent with the assumption that they come from K_SK_S decays. Furthermore, if we assume that all the ambiguous events in reaction (2) are truly $K^0\bar{K}^0\Delta^{++}$ events, then we obtain, after corrections, 53 ± 10. Neglecting phase-space corrections, we would expect a $C=+1$ state decaying into $K\bar{K}$ to go $\frac{1}{2}$ of the time into K^+K^-, $\frac{1}{4}$ into K_SK_S, and $\frac{1}{4}$ into K_LK_L. From the K^+K^- events (after a 7.2% phase-space correction) we expect 68 ± 6 K_SK_S events to be compared with the 53 ± 10 calculated from $K^0\bar{K}^0$ events. The agreement is reasonably good, indicating that less than 15% of the K^+K^- events in this region may come from a $C=-1$ state.

To compute the $\pi^+\pi^- \to K\bar{K}$ we simply multiplied the ratio of $K^+K^-\Delta^{++}$ events to $\pi^+\pi^-\Delta^{++}$ events by twice the extrapolated $\pi\pi$ cross section. The results include a phase-space correction for the difference in mass between K^0 and K^+.

IV. ENERGY-DEPENDENT ANALYSIS: METHOD

The partial-wave amplitudes for $\pi^+\pi^-$ scattering may be written as

$$S=\tfrac{2}{3}T_0^0+\tfrac{1}{3}T_0^2,\quad P=T_1^1,$$
$$D=\tfrac{2}{3}T_2^0+\tfrac{1}{3}T_2^2,\quad F=T_3^1, \tag{4.1}$$

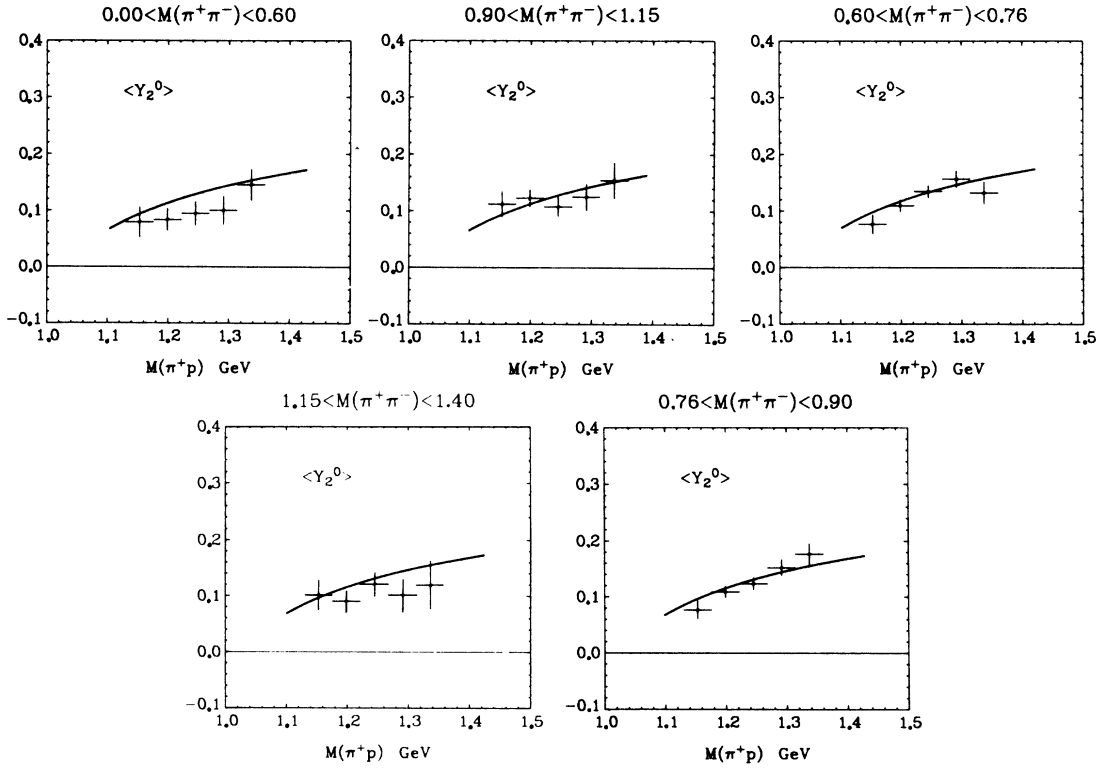

FIG. 10. Extrapolated $\langle Y_2^0\rangle$ moments for π^+p vertex. Curves correspond to physical π^+p scattering.

TABLE II. Parametrization of partial waves.

Partial wave	Parametrization	Number of free parameters
$I=0$ s wave	2×2 M matrix coupling $\pi\pi$ and $K\bar{K}$ channels	7
$I=1$ p wave [a]	ρ resonance + background, both become inelastic at 900 MeV	7
$I=0$ d wave [a]	f_0 resonance coupled to $\pi\pi$ and $K\bar{K}$ + background which becomes inelastic at 900 MeV	5
$I=1$ f wave [a]	Elastic g resonance + background which becomes inelastic at 900 MeV	5
$I=2$ s wave	$\eta_2^0=1$, $\delta_2^0=q\sum_{n=0}^{5} c_n q^{2n}$	0
$I=2$ d wave	$\eta_2^2=1$, $\delta_2^2=aq^2$	0

[a] Parametrization for this wave is similar to one used by Roper, Wright, and Feld (Ref. 18) to calculate πN phase shifts.

where

$$T_l^I=\frac{1}{2i}(\eta_l^I e^{2i\delta_l^I}-1)\ . \tag{4.2}$$

Upper indices denote isospin, and lower indices angular momentum l. The cross section and the Y_L^0 moments are, in terms of the above amplitudes,

$$\sigma_{\pi\pi}=4\pi\lambda^2(|S|^2+3|P|^2+5|D|^2+7|F|^2)\ ,$$

$$\langle Y_1^0\rangle=\left[\left(\frac{3}{\pi}\right)^{1/2}\mathrm{Re}(S^*P)+2\left(\frac{3}{\pi}\right)^{1/2}\mathrm{Re}(P^*D)+3\left(\frac{3}{\pi}\right)^{1/2}\mathrm{Re}(D^*F)\right]\frac{4\pi\lambda^2}{\sigma_{\pi\pi}}\ ,$$

$$\langle Y_2^0\rangle=\left[\frac{3}{(5\pi)^{1/2}}|P|^2+\left(\frac{5}{\pi}\right)^{1/2}\mathrm{Re}(S^*D)+\frac{5}{7}\left(\frac{5}{\pi}\right)^{1/2}|D|^2+\frac{9}{(5\pi)^{1/2}}\mathrm{Re}(P^*F)+\frac{14}{3(5\pi)^{1/2}}|F|^2\right]\frac{4\pi\lambda^2}{\sigma_{\pi\pi}}\ ,$$

$$\langle Y_3^0\rangle=\left[\frac{9}{(7\pi)^{1/2}}\mathrm{Re}(P^*D)+\frac{4}{3}\left(\frac{7}{\pi}\right)^{1/2}\mathrm{Re}(D^*F)+\left(\frac{7}{\pi}\right)^{1/2}\mathrm{Re}(S^*F)\right]\frac{4\pi\lambda^2}{\sigma_{\pi\pi}}\ , \tag{4.3}$$

$$\langle Y_4^0\rangle=\left[\frac{15}{7\sqrt{\pi}}|D|^2+\frac{4}{\sqrt{\pi}}\mathrm{Re}(P^*F)+\frac{21}{11\sqrt{\pi}}|F|^2\right]\frac{4\pi\lambda^2}{\sigma_{\pi\pi}}\ ,$$

$$\langle Y_5^0\rangle=\frac{50}{3(11\pi)^{1/2}}\mathrm{Re}(D^*F)\frac{4\pi\lambda^2}{\sigma_{\pi\pi}}\ ,$$

$$\langle Y_6^0\rangle=\frac{350}{33(13\pi)^{1/2}}|F|^2\frac{4\pi\lambda^2}{\sigma_{\pi\pi}}\ .$$

The total number of parameters [Eqs. (4.1) and (4.2)] to be determined at each value of $m_{\pi\pi}$ is 12, assuming partial waves up to $L=3$ are important. It is not possible to determine them by an energy-independent analysis using the reaction $\pi^+p\to\pi^+\pi^-\Delta^{++}$ alone,[15] since we only have seven constraints – six moments and the cross section [Eq. (4.3)]. In order to extract phases and inelasticities we parametrize them as functions of $\pi\pi$ mass (or momentum) and then do a least-squares fit to the moments and the cross section.

The parametrization we use is the following (summarized in Table II).

A. p Wave, f Wave, and $I=0$ d Wave

For the $I=1$ p wave and f wave, and the $I=0$ d wave, we use a background, T_B, plus a Breit-Wigner amplitude f_{BW},

$$T_l^I=\frac{\eta_B^{(l)}e^{2i\delta_B^{(l)}}-1}{2i}+e^{2i\phi^{(l)}}f_{\mathrm{BW}}^{(l)}\ , \tag{4.4}$$

where

$$\eta_B^{(I)} = \begin{cases} 1 \text{ below } \omega\pi \text{ threshold} \\ e^{-\nu^{(I)}} \text{ above } \omega\pi \text{ threshold,} \end{cases}$$

$$\nu^{(I)} = (q - q_{\text{th}})^{2I+1}\left(\sum_{n=0}^{1} b_n^{(I)} q^n\right)^2 , \tag{4.5}$$

$$\delta_B^{(I)} = q^{2I+1}\sum_{n=0}^{N} (a_n^{(I)} q^n) , \tag{4.6}$$

$q = \pi\pi$ c.m. momentum ,

$q_{\text{th}} = q$ evaluated at $\omega\pi$ threshold ,

$$f_{\text{BW}}^{(I)} = \frac{\Gamma_{\pi\pi}^{(I)}/2}{E_R^{(I)} - E - (i\,\Gamma^{(I)}/2)} , \tag{4.7}$$

$$\Gamma_{\pi\pi}^{(I)} = \Gamma_R^{(I)}\left(\frac{q}{q_R^{(I)}}\right)^{2I+1} \frac{2E_R^{(I)}}{E_R^{(I)} + E} \frac{D_I^R}{D_I} , \tag{4.8}$$

$E = \pi\pi$ c.m. energy ,

$q_R^{(I)} = q$ evaluated at $E = E_R$,

$D_I^R = D_I$ evaluated at $E = E_R$.

For the p wave,

$$\Gamma^{(1)} = \Gamma_{\pi\pi}^{(1)} + \Gamma_{\omega\pi} ,$$

$$D_1 = 1 + q^2 r_\rho{}^2 , \tag{4.9}$$

$$\Gamma_{\omega\pi} = \begin{cases} 0 \text{ below } \omega\pi \text{ threshold} \\ g_{\omega\rho\pi}{}^2 q_{\omega\pi}{}^3 \text{ above } \omega\pi \text{ threshold.} \end{cases}$$

There are eight parameters describing this wave that must be obtained from the fit, namely, $a_0^{(1)}$, $a_1^{(1)}$, $b_0^{(1)}$, $b_1^{(1)}$, $\Gamma_R^{(1)}$, $E_R^{(1)}$, $g_{\rho\omega\pi}$, and r_ρ. It turns out that $g_{\rho\omega\pi}$ is strongly correlated with $b_0^{(1)}$ and $b_1^{(1)}$, so $g_{\rho\omega\pi}{}^2$ was fixed[16] at 0.6 GeV^{-2} and only seven parameters were allowed to vary.

For the d wave,

$$\Gamma^{(2)} = \Gamma_{\pi\pi}^{(2)} + \Gamma_{K\bar{K}} ,$$

$$D_2 = 9 + 3q^2 r_f{}^2 + q^4 r_f{}^4 ,$$

$$\Gamma_{\bar{K}K} = \begin{cases} 0 \text{ below } K\bar{K} \text{ threshold} \\ g_{K\bar{K}}{}^2 (q_{K\bar{K}}/q_{K\bar{K}}^R)^5 \text{ above } K\bar{K} \text{ threshold} , \end{cases} \tag{4.10}$$

$q_{K\bar{K}}$ = c.m. momentum of $K\bar{K}$ system ,

$q_{K\bar{K}}^R = q_{K\bar{K}}$ at $E = E_R^{(2)}$.

In this case, since the over-all fit is only up to 1.15 GeV, $\Gamma_R^{(2)}$, $E_R^{(2)}$, and r_f are kept fixed at values obtained from a fit to the mass distribution alone ($\Gamma_R^{(2)} = 0.18$ GeV, $E_R^{(2)} = 1.28$ GeV, $r_f = 1.1$ GeV^{-1}), and $g_{K\bar{K}}{}^2$ is set at 0.03 GeV. This value was chosen by comparing the number of events in the $K\bar{K}$ channel to the number of events in the $\pi^+\pi^-$ channel in the f_0 region for $|t'| < 0.1$ GeV^2. At such low t the A_2 contribution to $K\bar{K}$ in that mass region should be quite small. The fits are not particularly sensitive to the value of $g_{KK}{}^2$ as long as $g_{K\bar{K}}{}^2 < 0.1$. The parameters left free are five: $a_0^{(2)}$, $a_1^{(2)}$, $a_2^{(2)}$, $b_0^{(2)}$, and $b_1^{(2)}$.[17]

For the f wave we use an elastic g resonance (fixed mass and width) plus a background with five parameters: $a_0^{(3)}$, $a_1^{(3)}$, $a_2^{(3)}$, $b_0^{(3)}$, and $b_1^{(3)}$.

The parametrization for the p wave, f wave, and $I = 0$ d wave has the expected threshold behavior for δ and is a reasonable approximation for η. In addition it is a good approximation to the expected behavior of an inelastic resonance plus inelastic background in the elastic channel if the pole is not close to a threshold.[18] For certain values of $\phi^{(I)}$ the parametrization may violate unitarity at some energies. We found that in setting $\phi^{(I)} = \delta_B^{(I)}$, unitarity was never violated in the fitted region. We emphasize that we are not attempting to separate the amplitude into background plus a resonance, we are simply using what we consider a reasonable approximation to the dependence of δ and η on the energy in order to extract them from the data. No particular significance should be attached to the values obtained for the parameters themselves.

B. $I = 2$ s and d Waves

The fits are not very sensitive to the $I = 2$ amplitudes, which are known to be fairly small in the fitted region. We set $\eta_0^2 = \eta_2^2 = 1$ throughout. For the $I = 2$ s wave we take

$$\delta_0^2 = q\sum_{n=0}^{5} C_n q^{2n} ,$$

where the various coefficients were obtained by fitting published data.[19]

The δ_2^2 phase is poorly known at present but is believed to be negative.[20] For the $I = 2$ d wave we set

$$\delta_2^2 = aq^5 ,$$

where $a = -100$ GeV^{-5}. This reproduces reasonably well the values given by Baton *et al.*[14]

C. $I = 0$ s Wave

The $I = 0$ s-wave amplitude is parametrized in terms of a 2×2 M matrix[21]; we assume that only the $\pi\pi$ and $K\bar{K}$ channels are important. Assuming that most of the events in $\pi^+\pi^-\pi^0\pi^0$ below 1 GeV come from $\omega\pi$ events, we can estimate (see Figs. 3 and 4) that below the $K\bar{K}$ threshold $\eta_0^0 \gtrsim 0.98$. Thus a two-channel analysis should be adequate for this wave.

Set

$$T_0^0 = \begin{pmatrix} T_{11} & T_{12} \\ T_{12} & T_{22} \end{pmatrix},$$

where

$T_{11} = \pi\pi \to \pi\pi$ s-wave amplitude,

$T_{12} = \pi\pi \to K\bar{K}$ s-wave amplitude,

$T_{22} = K\bar{K} \to K\bar{K}$ s-wave amplitude.

These amplitudes are normalized so that

$$\sigma_{ij} = 4\pi\lambda^2 |T_{ij}|^2 .$$

In terms of the M matrix,

$$T = k^{1/2}(M - ik)^{-1}k^{1/2} ,$$

k = diagonal matrix of momenta.

Explicitly, T is given by

$$T = \frac{1}{D}\begin{pmatrix} k_1(M_{22} - ik_2) & -(k_1k_2)^{1/2}M_{12} \\ -(k_1k_2)^{1/2}M_{12} & k_2(M_{11} - ik_1) \end{pmatrix} , \qquad (4.11)$$

where

$$D = (M_{11} - ik_1)(M_{22} - ik_2) - M_{12}^2 ,$$

$k_1 = \pi$ momentum in $\pi\pi$ rest frame ,

$k_2 = K$ momentum in $K\bar{K}$ rest frame .

This representation – provided M is real and symmetric – with the prescription $k_2 \to i|k_2|$ below $K\bar{K}$ threshold satisfies the requirements of analyticity and unitarity under the assumption that we can neglect channels other than $\pi\pi$ and $K\bar{K}$. The M-matrix elements are taken of the form

$$M_{ij} = M_{ij}^0 + M_{ij}^1(s - s_0) , \qquad (4.12)$$

where $s = m_{\pi\pi}^2$ and $s_0 = s$ at $K\bar{K}$ threshold. It is evident that the results are independent of the choice of s_0. A reasonable fit can be obtained with a linear expansion of M_{ij}, but χ^2 improves substantially if one more term is added to either M_{12} or M_{22}. Adding more terms only increases the correlations between parameters without changing χ^2 significantly. So we use a linear expansion in M_{11} and M_{22} and a quadratic one in M_{12}. This gives seven free parameters for the $I = 0$ s-wave amplitude. From the data in the physical region (for which we have ±8-MeV resolution, full width at half maximum), we can infer that the s-wave amplitude should be almost zero within 10 MeV of $K\bar{K}$ threshold, and one could force that constraint on the fit by setting $M_{22}^0 = 0$.

V. ENERGY-DEPENDENT ANALYSIS: SOLUTIONS

We have 24 parameters to be determined from the data. The parametrization is summarized in Table II. We fit the extrapolated moments up to Y_6^0 and the cross sections ($\pi^+\pi^- \to \pi^+\pi^- \to K\bar{K}$) between 550 and 1150 MeV with a total of 171 points.[22] We did a large number of fits starting from different initial values and varying slightly the pa-

TABLE III. Properties of three different fits.[a]

Case	Description	Degrees of freedom	χ^2	S^* pole (MeV)	ϵ pole (MeV)
1	Background phase for $l \neq 0$ waves given by $\delta_B^{(I)} = q^{2l+1}\sum_{n=0}^{N} a_n^{(I)} q^n$	147	164.6	$997 \pm 6 - i(27 \pm 8)$	$660 \pm 100 - i(320 \pm 70)$
	M-matrix elements			II sheet	II sheet
	$M_{ij} = M_{ij}^0 + M_{ij}^1(s - s_0) + M_{ij}^2(s - s_0)^2$				
	See text for complete description				
2	Background phase for $l \neq 0$ waves given by $\delta_B^{(I)} = q^{2l+1}D_l^{-1}(q)\sum_{n=0}^{N} a_n^{(I)} q^n$	147	164.4	$982 \pm 6 - i(37 \pm 8)$	See text
	M-matrix elements			II sheet	See text
	$M_{ij} = M_{ij}^0 + M_{ij}^1(E - E_0) + M_{ij}^2(E - E_0)^3$				
	Otherwise same as case 1				
3	Same as case 1 but only four parameters for s wave	150	173.0	$996 \pm 7 - i(52 \pm 8)$	No ϵ pole

[a] In all 3 fits Eq. 5.1 was used for η_3^1.

rametrization for each of the waves. We must emphasize that our parametrization is by no means unique and other parametrizations might serve equally well. Variations in our parametrization are discussed later on. The χ^2 for the best fits range from 164 to 173, which for 147 degrees of freedom corresponds to confidence levels between 16% and 7%. In Table III we list some properties of the three fits with similar χ^2 which differed the most. The curves shown on Fig. 8 are for case 1; the parameters and error matrix for this case are given in Tables IV and V.

Overall the fit seems reasonably good, but there are some noticeable discrepancies. Between 550 and 650 MeV, the predicted Y_1^0 is systematically high, Y_2^0 is systematically low, and Y_4^0 is not as negative as the data. It might be possible to improve the fit if the f wave is more negative in that region than the present parametrization permits. In the region 760 to 800 MeV the $\pi\pi$ cross section and Y_1^0 have a dip and Y_2^0 a spike not predicted by the fit. If we believe that in that region only s and p waves are important, then the value for extrapolated Y_2^0 is unphysical. The contribution to χ^2 of that region is 32 (for nine points), so it was excluded from the final fits. Since this effect occurs very close to the ω mass (783 MeV), it is certainly possible that it is associated with ρ-ω interference. If this is the case it is somewhat surprising that we observe the effect on the extrapolated data, since the ω cannot be produced by π exchange (at least not strongly); thus, it is part of the background that should disappear when we extrapolate. On the contrary, the extrapolation enhances the effect. A similar phenomenon was observed in the extrapolation of $\pi\pi$ cross section by Colton *et al.*[23] for the reaction $\pi^+p \to \pi^+\pi^-\Delta^{++}$ at 8 GeV/c. To see if this enhancement was due simply to the conditions of the extrapolation [i.e., linear and including events up to $|t_{p\Delta}| = 0.4$ (GeV/c)^2] we performed quadratic and linear extrapolations using different cutoffs for t in that region. The quadratic extrapolations tend to enhance the effect even more; choosing smaller cutoffs only increased errors without changing results significantly. An explanation for this effect, which is consistent with data for reaction $\pi^+p \to \omega\Delta^{++}$ at 7.1 GeV/c, is that at small t the ω is produced mainly by B exchange with zero helicity. In this case ρ-ω interference is most pronounced at small t, distorting results of extrapolation to the π pole. See Sec. VII C for more details on this effect.

TABLE IV. Parameters obtained from fit (case 1).[a]

$I=0$ s wave	$M_{11}^0 = -1.05 \pm 2.2$	$M_{11}^1 = -0.087 \pm 0.33$	
	$M_{12}^0 = 1.93 \pm 0.42$	$M_{12}^1 = +0.205 \pm 0.24$	$M_{12}^2 = 0.0031 \pm 0.0007$
	$M_{22}^0 = 0.043 \pm 0.06$	$M_{22}^1 = -0.241 \pm 0.25$	
$I=1$ p wave	$E_R^{(1)} = 0.775 \pm 0.004$ GeV	$\Gamma_R^{(1)} = 0.160 \pm 0.01$ GeV	$r_\rho = 3.0 \pm 0.9$ GeV^{-1}
	$a_0^{(1)} = 0.19 \pm 0.25$	$a_1^{(1)} = -0.034 \pm 0.064$	
	$b_0^{(1)} = 2.215 \pm 3.0$	$b_1^{(1)} = -0.611 \pm 0.7$	
$I=0$ d wave	$a_0^{(2)} = -0.18 \pm 0.09$	$a_1^{(2)} = 0.095 \pm 0.05$	$a_2^{(2)} = -0.012 \pm 0.008$
	$b_0^{(2)} = 20.0 \pm 4.8$	$b_1^{(2)} = -5.0 \pm 1.2$	
$I=1$ f wave	$a_0^{(3)} = -0.093 \pm 0.006$	$a_1^{(3)} = 0.0043 \pm 0.003$	$a_2^{(3)} = -0.0005 \pm 0.0004$
	$b_0^{(3)} = 2.31 \pm 0.27$	$b_1^{(3)} = -6.27 \pm 1.83$	
$I=2$ d wave	$a = -100$ GeV^{-5} (fixed)		
$I=2$ s wave	$c_0 = -2.2 \times 10^{-2}$	$c_1 = -4.17 \pm 10^{-2}$	$c_2 = 1.48 \times 10^{-2}$ $c_3 = -2.49 \times 10^{-3}$
	$c_4 = 1.76 \times 10^{-4}$	$c_5 = -4.24 \times 10^{-6}$	(all fixed)

[a] Correlations between parameters are large; for any computation using these parameters the full error matrix should be used (Table V). Unless otherwise indicated, units are in appropriate powers of μ (π mass).

TABLE V. Normalized error matrix $[E_{ij} = \langle \delta x_i \delta x_j \rangle / (\langle \delta x_i^2 \rangle \langle \delta x_j^2 \rangle)^{1/2}]$.

	M_{11}^0	M_{12}^0	M_{11}^1	M_{12}^1	M_{22}^1	M_{12}^2	M_{22}^0	$a_0^{(1)}$	$a_1^{(1)}$	$E_R^{(1)}$	$\Gamma_R^{(1)}$	r_p	$a_0^{(2)}$	$a_1^{(2)}$	$a_2^{(2)}$	$a_0^{(3)}$	$a_1^{(3)}$	$b_0^{(1)}$	$b_1^{(1)}$	$a_2^{(3)}$	$b_0^{(2)}$	$b_1^{(2)}$	$b_0^{(3)}$	$b_1^{(3)}$
M_{11}^0	1.00	−0.85	1.00	−0.99	0.95	0.93	−0.19	0.06	−0.04	0.06	0.16	−0.05	−0.14	0.13	−0.12	−0.04	0.03	−0.04	0.05	−0.02	0.10	−0.09	0.07	−0.15
M_{12}^0	−0.85	1.00	−0.84	0.87	−0.91	−0.81	−0.06	−0.08	0.07	−0.05	−0.08	0.03	0.16	−0.17	0.17	−0.02	0.04	−0.02	0.02	−0.05	−0.04	0.04	0.04	−0.00
M_{11}^1	1.00	−0.84	1.00	−1.00	0.95	0.92	−0.17	0.07	−0.04	0.06	0.16	−0.05	−0.14	0.14	−0.12	−0.05	0.03	−0.03	0.05	−0.02	0.10	−0.10	0.07	−0.15
M_{12}^1	−0.99	0.87	−1.00	1.00	−0.97	−0.92	0.17	−0.07	0.05	−0.05	−0.15	0.04	0.15	−0.15	0.14	0.04	−0.03	0.02	−0.03	0.01	−0.09	0.09	−0.06	0.13
M_{22}^1	0.95	−0.91	0.95	−0.97	1.00	0.89	−0.17	0.07	−0.06	0.04	0.11	−0.01	−0.17	0.17	−0.17	−0.02	0.01	0.01	−0.01	−0.01	0.06	−0.05	0.01	−0.06
M_{12}^2	0.93	−0.81	0.92	−0.92	0.89	1.00	−0.28	0.05	−0.04	0.02	0.05	−0.02	−0.09	0.09	−0.09	−0.05	0.04	−0.01	0.02	−0.03	0.08	−0.08	0.04	−0.11
M_{22}^0	−0.19	−0.06	−0.17	0.17	−0.17	−0.28	1.00	0.08	−0.08	0.03	−0.03	−0.07	−0.07	0.09	−0.11	0.03	−0.04	0.05	−0.05	0.05	0.07	−0.07	−0.02	0.06
$a_0^{(1)}$	0.06	−0.08	0.07	−0.07	0.07	0.05	0.08	1.00	−0.98	0.75	0.11	−0.66	−0.26	0.25	−0.24	0.13	−0.15	0.33	−0.24	0.16	0.27	−0.26	−0.30	0.28
$a_1^{(1)}$	−0.04	0.07	−0.04	0.05	−0.06	−0.04	−0.08	−0.98	1.00	−0.64	0.06	0.52	0.27	−0.27	0.27	−0.11	0.13	−0.39	0.31	−0.14	−0.20	0.19	0.28	−0.25
$E_R^{(1)}$	0.06	−0.05	0.06	−0.05	0.04	0.02	0.03	0.75	−0.64	1.00	0.58	−0.56	−0.19	0.17	−0.15	0.12	−0.14	0.03	0.03	0.14	0.28	−0.28	−0.19	0.19
$\Gamma_R^{(1)}$	0.16	−0.08	0.16	−0.15	0.11	0.05	−0.03	0.11	0.06	0.58	1.00	−0.34	−0.15	0.11	−0.07	0.06	−0.07	−0.19	0.20	0.07	0.28	−0.28	−0.09	0.10
r_p	−0.05	0.03	−0.05	0.04	−0.01	−0.02	−0.07	−0.66	0.52	−0.56	−0.34	1.00	−0.01	0.02	−0.04	−0.17	0.19	−0.20	0.11	−0.20	−0.44	0.43	0.41	−0.39
$a_0^{(2)}$	−0.14	0.16	−0.14	0.15	−0.17	−0.09	−0.07	−0.26	0.27	−0.19	−0.15	−0.01	1.00	−0.99	0.98	−0.16	0.16	−0.33	0.33	−0.17	−0.19	0.19	0.10	−0.14
$a_1^{(2)}$	0.13	−0.17	0.14	−0.15	0.17	0.09	0.09	0.25	−0.27	0.17	0.11	0.02	−0.99	1.00	−0.99	0.15	−0.16	0.37	−0.37	0.16	0.19	−0.19	−0.11	0.17
$a_2^{(2)}$	−0.12	0.17	−0.12	0.14	−0.17	−0.09	−0.11	−0.24	0.27	−0.15	−0.07	−0.04	0.98	−0.99	1.00	−0.14	0.15	−0.40	0.41	−0.16	−0.18	0.19	0.13	−0.20
$a_0^{(3)}$	−0.04	−0.02	−0.05	0.04	−0.02	−0.05	0.03	0.13	−0.11	0.12	0.06	−0.17	−0.16	0.15	−0.14	1.00	−1.00	0.12	−0.11	0.99	0.08	−0.07	−0.15	0.13
$a_1^{(3)}$	0.03	0.04	0.03	−0.03	0.01	0.04	−0.04	−0.15	0.13	−0.14	−0.07	0.19	0.16	−0.16	0.15	−1.00	1.00	−0.13	0.11	−1.00	−0.09	0.08	0.19	−0.16
$b_0^{(1)}$	−0.04	−0.02	−0.03	0.02	0.01	−0.01	0.05	0.33	−0.39	0.03	−0.19	−0.20	−0.33	0.37	−0.40	0.12	−0.13	1.00	−0.99	0.13	0.07	−0.07	−0.17	0.29
$b_1^{(1)}$	0.05	0.02	0.05	−0.03	−0.01	0.02	−0.05	−0.24	0.31	0.03	0.20	0.11	0.33	−0.37	0.41	−0.11	0.11	−0.99	1.00	−0.12	−0.03	0.03	0.14	−0.28
$b_0^{(2)}$	−0.00	−0.05	−0.02	0.01	0.01	−0.03	0.05	0.16	−0.14	0.14	0.07	−0.20	−0.17	0.16	−0.16	0.99	−1.00	0.13	−0.12	1.00	0.10	−0.09	−0.21	0.18
$b_1^{(2)}$	0.10	−0.04	0.10	−0.09	0.06	0.08	0.07	0.27	−0.20	0.28	0.28	−0.44	−0.19	0.19	−0.18	0.09	−0.09	0.07	−0.03	0.10	1.00	−1.00	−0.27	0.12
$a_2^{(3)}$	−0.09	0.04	−0.10	0.09	−0.05	−0.08	−0.07	−0.26	0.19	−0.28	−0.28	0.43	0.19	−0.19	0.19	−0.07	0.08	−0.07	0.03	−0.09	−1.00	1.00	0.26	−0.11
$b_0^{(3)}$	0.07	0.04	0.07	−0.06	0.01	0.04	−0.02	−0.30	0.28	−0.19	−0.09	0.41	0.10	−0.11	0.13	−0.15	0.19	−0.17	0.14	−0.21	−0.27	0.26	1.00	−0.90
$b_1^{(3)}$	−0.15	−0.00	−0.15	0.13	−0.06	−0.11	0.06	0.28	−0.25	0.19	0.10	−0.39	−0.14	0.17	−0.20	0.13	−0.16	0.29	−0.28	0.18	0.12	−0.11	−0.90	1.00

In order to fit the moments Y_3^0 to Y_6^0 above 900 MeV, we needed all waves (excluding $l=0$ and $I=2$ amplitudes) to become inelastic at the $\omega\pi$ threshold.[17] If the ω had zero width this threshold would be at 920 MeV; the fits improved somewhat if we allowed the threshold to start at 900 MeV instead. We also found that we could not fit very well the moments Y_4^0 to Y_6^0 with the parametrization for η_3^1 described earlier [Eq. (4.5)]. In addition, by 1.0 GeV, η_3^1 was too small to be consistent with data in the 4π channels (predicting an order-of-magnitude more events than observed). A better fit is obtained if we take instead

$$\eta_B^{(3)}=\frac{1}{1+(q-q_{\rm th}}\,\frac{1}{b_0^{(3)}+b_1^{(3)}q)^2}\quad\text{above }\omega\pi\text{ threshold},\qquad(5.1)$$

$$\eta_B^{(3)}=1\quad\text{below }\omega\quad\text{threshold}.$$

We still obtain η_3^1 inconsistent with other channels, and in addition the above parametrization does not have the correct threshold behavior. This is an undesirable feature of our fit but cannot be avoided. A likely explanation is that the f wave is being used to fit non-π-exchange background in that region and is not the true $\pi\pi$ f-wave amplitude. If the extrapolation for some reason (either background or absorption effects) gives values for the moments above 900 MeV that are higher than the true physical moments, then the easiest way to correct for that failure is to introduce a purely imaginary f-wave amplitude, since such a term would give a positive contribution to all the moments. We must point out though that results obtained for the p and s waves are little affected by this complication.[24] As long as we believe that the rapidly varying features in our data are due to the behavior of these waves (s and p), while the other waves are fairly smooth, the values obtained for s and p waves cannot change by much regardless of how the other waves are parametrized. This indeed was observed for the different fits attempted. We therefore feel confident that the general features of the $I=0$ s wave and $I=1$ p wave between 550 and 1000 MeV have been well determined by our fit.[25] Above 1.0 GeV our values are in disagreement with values reported in other experiments.[26,27] Our fit to the $K\bar{K}$ cross section is somewhat poor, the predicted values being systematically lower than the observed ones. The fit improves substantially if all the observed inelasticity in the d wave is assumed to contribute to the $K\bar{K}$ channel. However, the $K\bar{K}$ moments do not seem consistent with much d wave in that region (see Ref. 2). It is thus possible that the discrep-

TABLE VI. Phases (in degrees) and inelasticities (case 1).

Mass (GeV)	δ_0^0	η_0^0	δ_1^1	η_1^1	δ_2^0	η_2^0	δ_3^1	η_3^1
0.55	43 ± 2		10 ± 0.7		0 ± 0.5		0 ± 0.1	
0.625	56 ± 3		19 ± 0.8		0 ± 0.5		−0.4 ± 0.2	
0.665	62 ± 4		30 ± 1		0 ± 0.5		−0.5 ± 0.2	
0.690	68 ± 4		39 ± 1		0 ± 0.5		−0.6 ± 0.3	
0.71	69 ± 4		48 ± 1		0 ± 0.5		−0.8 ± 0.4	
0.73	72 ± 4		60 ± 1.5		0 ± 0.5		−0.8 ± 0.4	
0.745	74 ± 4		70 ± 1.5		0 ± 0.5		−0.9 ± 0.4	
0.755	76 ± 4		77 ± 1.6		0 ± 0.5		−0.0 ± 0.4	
0.765	77 ± 4		85 ± 1.6		0 ± 0.5		−1.0 ± 0.4	
0.775	79 ± 4		92 ± 1.6		0 ± 0.5		−1.0 ± 0.4	
0.785	80 ± 4		99 ± 1.5		0 ± 0.5		−1.0 ± 0.4	
0.795	81 ± 4		105 ± 1.5		0 ± 0.5		−1.1 ± 0.4	
0.810	83 ± 4		114 ± 1.4		0.4 ± 1		−1.2 ± 0.5	
0.83	86 ± 4		124 ± 1.2		1.0 ± 0.9		−1.3 ± 0.5	
0.85	88 ± 3.5		131 ± 1.1		1.6 ± 1		−1.4 ± 0.5	
0.87	91 ± 4		136 ± 1		2.5 ± 1		−1.4 ± 0.5	
0.89	94 ± 4		142 ± 0.8		3.3 ± 1		−1.5 ± 0.5	
0.91	99 ± 4		145 ± 0.8		4.4 ± 1		−1.5 ± 0.5	0.95 ± 0.02
0.935	109 ± 5		150 ± 0.9	0.99 ± 0.01	6.4 ± 1.2	0.99 ± 0.01	−1.4 ± 0.5	0.85 ± 0.05
0.965	134 ± 5.5		153 ± 1	0.99 ± 0.01	8.9 ± 1.4	0.99 ± 0.01	−1.1 ± 0.6	0.80 ± 0.05
1.0	194 ± 9	0.39 ± 0.08	156 ± 1.2	0.99 ± 0.01	12 ± 2	0.94 ± 0.03	−0.7 ± 0.8	0.78 ± 0.05
1.04	215 ± 9	0.35 ± 0.04	158 ± 1.6	0.99 ± 0.03	19 ± 2.5	0.84 ± 0.06	0.1 ± 0.7	0.78 ± 0.05
1.075	215 ± 8	0.42 ± 0.04	160 ± 2.5	0.98 ± 0.05	27 ± 4	0.78 ± 0.08	1.2 ± 0.8	0.80 ± 0.05
1.105	213 ± 8	0.48 ± 0.04	162 ± 3.4	0.98 ± 0.06	34 ± 4	0.81 ± 0.06	2.4 ± 1.1	0.82 ± 0.06
1.135	210 ± 8	0.54 ± 0.04	163 ± 4	0.96 ± 0.06	40 ± 5	0.91 ± 0.04	3.8 ± 1.8	0.86 ± 0.07
1.150	208 ± 7	0.57 ± 0.04	164 ± 6	0.94 ± 0.07	44 ± 7	0.94 ± 0.04	4.5 ± 2.0	0.90 ± 0.1

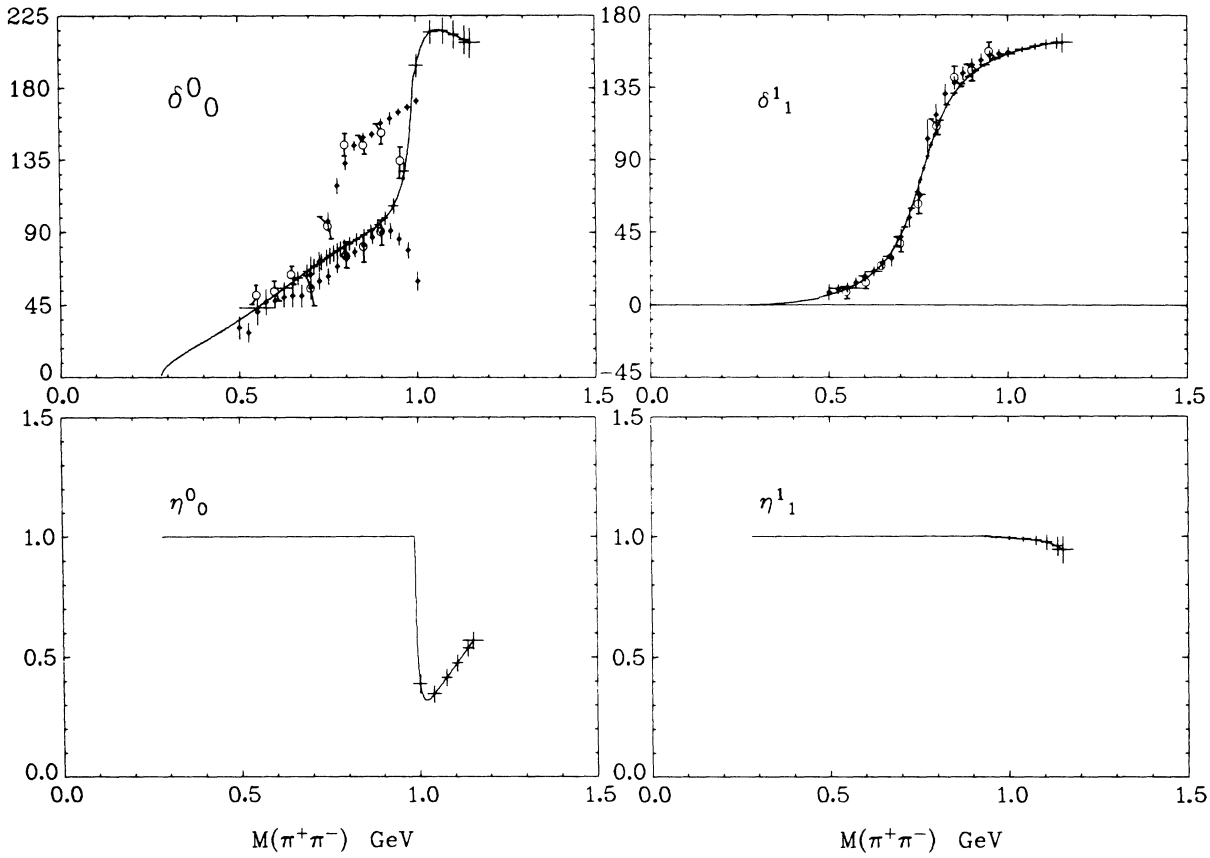

FIG. 11. Phases and inelasticities of $I=0$ s wave and $I=1$ p wave. The crosses are the points calculated from our data. The horizontal bars of the crosses give size of bins used in the fit to the moments and cross section. The vertical bars indicate the calculated error at a given mass. These errors are purely statistical and do not reflect possible systematic effects introduced by extrapolation procedure. The dots correspond to the elastic "down" and "up" solutions of Baton, Laurens, and Reignier (Ref. 26). The open circles are the results of Baillon *et al.* (Ref. 27).

ancy is due either to non-π-exchange background or to our crude estimate of the $K\bar{K}$ cross section (see Sec. III C).

With the parameters obtained from our fit we can compute the phases and inelasticities. These are tabulated in Table VI and shown in Figs. 11 and 12 for case 1 (see Table IV). We point out that the given errors are computed by standard propagation of error and reflect only the statistical errors; they do not reflect the inherent uncertainties in performing an extrapolation. They should be considered only as an indication of the minimum error in our computed values. How accurate our results really are can only be ascertained by comparison with results of an experiment at different energy with comparable statistics.

For the p-wave phase shift (δ^1_1) we obtain the well-known Breit-Wigner shape (with $\delta^1_1=90°$ at 0.772 GeV, $\delta^1_1=45°$ at 0.703 GeV, and $\delta^1_1=135°$ at 0.863 GeV); the inelasticity (η^1_1) is close to unity within errors, although by 1.13 GeV it could be as small as 0.8. The $I=0$ d-wave phase shift (δ^0_2) around 1 GeV is larger than we would expect for the f_0 meson alone. This wave also seems to be quite inelastic ($\eta^0_2 \approx 0.80$ at 1.070 GeV). This result has to be viewed with caution because it depends strongly on what is assumed for the f-wave inelasticity, and non-π-exchange background (or absorption) may have a substantial effect on these waves. The effect of the $I=2$ d wave (δ^2_2) is small; we can obtain a good fit by setting $\delta^2_2=0$ throughout. The f-wave phase shift is small and negative under the ρ and becomes positive past the $\omega\pi$ threshold. As indicated before, the obtained inelasticity is too small to be compatible with the data in the inelastic channels; we believe that it is simply acting as a parametrization of background (or a failure of the extrapolation). What bearing various effects may have on our results will be discussed in more detail in Sec. VII.

The most interesting results are the phase shift and inelasticity of the $I=0$ s wave. The phase

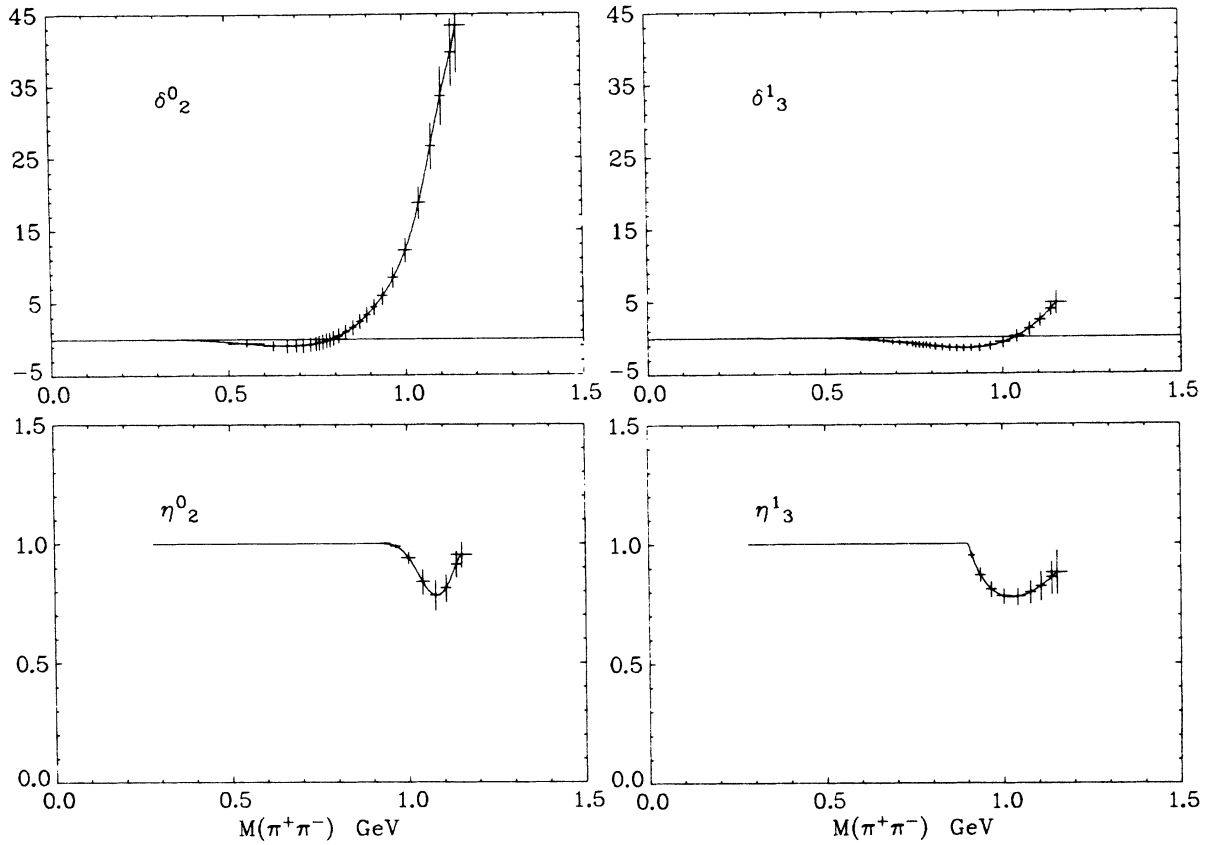

FIG. 12. Phases and inelasticities of $I=0$ d wave and $I=1$ f wave.

rises from 45° at 550 MeV to 75° at 740 MeV, then increases slowly until 950 MeV, crossing 90° around 900 MeV. The phase below 850 MeV is in very good agreement with the one favored by Morgan and Shaw[28] (referred to as "between-down" solution). Above 900 MeV it increases rapidly, reaching 180° close to the $K\bar{K}$ threshold. Past the $K\bar{K}$ threshold the inelasticity reaches a minimum very rapidly (within 20 MeV), and then both phase and inelasticity vary rather slowly. This is in good agreement with the conclusions reached by a qualitative analysis of our data in the physical region.[3] At this point we should remark that the structure in the $\pi\pi$ data requires the maximum contribution of the s wave to the $K\bar{K}$ cross section to occur within 30 MeV of the $K\bar{K}$ threshold. This is consistent with our K^+K^- cross section ($|t'_{p\Delta}| < 0.1$ GeV^2) and the extrapolated cross section obtained by Hyams *et al.*[29] (in particular, the set "$t\sigma$" = bt and "$t\sigma$" = $bt + ct^2$), but is not consistent with the $K^0\bar{K}^0$ cross section of Beusch *et al.* ($\pi^-p \to K^0\bar{K}^0n$ at 4 and 6.2 GeV/c),[30] which reaches the maximum at 1.07 GeV. Part of the discrepancy might be from the fact that the Beusch *et al.* data are $|t| < 0.5$ GeV^2, from differences in background for K^+K^- and $K^0\bar{K}^0$, and from the mass difference between K^+ and $\bar{K}^0$. This question deserves more careful study.[31]

We can draw some interesting conclusions, using our parametrization of the s-wave amplitude. We find that the amplitude T has two poles on the second Riemann sheet as a function of complex energy. One (S^*) is very close to $K\bar{K}$ threshold at $997 \pm 6 - i(27 \pm 8)$. The existence of a pole in this region was suggested from a K-matrix fit to the $K\bar{K}$ cross section by Hoang.[32] The other pole (ϵ) is quite far from the physical region, at $660 \pm 100 - i(320 \pm 70)$. Strictly speaking, we should say that there are four poles, since each one has a corresponding complex conjugate pole. Additional poles are also present; a more complete discussion is given in Appendix A. Note that for both S^* and ϵ a conventional Breit-Wigner parametrization will not be adequate: One is too close to $K\bar{K}$ threshold, the other is too far from the real axis. We also computed the residues at both poles, which are given in Table VII.

To check how dependent these results are on parametrization, we re-did the fits with a somewhat different one (case 2 in Table III). In this case we

TABLE VII. Pole parameters for case 1.

Pole position (MeV)	Residues [a] (units of π mass)	$\pi\pi$ scattering length
S^*, $997 \pm 6 - i(27 \pm 8)$, II sheet	$R_{11} \approx 1.23 - i0.29$ $R_{12} \approx 0.64 + i1.88$ $R_{22} \approx -2.85 + i1.27$	
ϵ, $660 - i(320 \pm 70)$, II sheet	$R_{11} \approx -5.80 + i4.91$ $R_{12} \approx -0.62 + i1.64$ $R_{22} \approx 0.06 + i0.40$	$(0.34 \pm 0.18) m_\pi^{-1}$

[a] Residues defined as $R_{ij} = [(s - s_0)/(k_i k_j)^{1/2}] T_{ij}(s_0)$, where $s_0 = s$ at pole position.

added barrier factors to the $l \neq 0$ waves, i.e.,

$$\delta_B^{(l)} = q^{2l+1} D_l^{-1}(q) \sum_{n=0}^{N} a_n q^n \ , \tag{5.2}$$

where the $D_l(q)$ functions are as defined in Sec. IV [Eqs. (4.9) and (4.10)]. For the M matrix we took, instead of Eq. (4.12),

$$M_{ij} = M_{ij}^0 + M_{ij}^1 (E - E_0) \ ,$$

where E is the c.m. energy and $E_0 = E$ at $K\bar{K}$ threshold. For M_{12} we added an extra term $M_{12}^2 (E - E_0)^3$. The best χ^2 with this parametrization was essentially the same (164.4 as compared with 164.6 for 147 degrees of freedom). The phases and inelasticities changed within the computed errors. We again obtain an S^* pole on the second Riemann sheet at $982 \pm 6 - i(37 \pm 8)$. But instead of the ϵ pole this solution has a pole on the IV sheet at $889 - i123$ and another on the I sheet at $829 - i268$. In addition, the behavior of the phase shift below 450 MeV is clearly pathological; it goes counterclockwise, being 180° at threshold instead of 0°. Both solutions are plotted from threshold to 1150 MeV in Fig. 13. Clearly case 2 is not an acceptable solution. However, it illustrates that one can obtain fits with almost identical phase shifts in the 550- to 1150-MeV region and strikingly different behavior outside the fitted region, and that accurate data below 550 MeV are indispensable to determine whether a faraway pole like the ϵ exists.

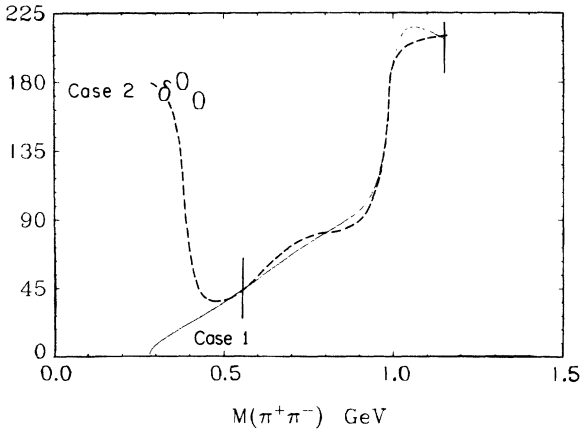

FIG. 13. Case-1 (solid line) and case-2 (dashed line) solutions for δ_0^0 (see Sec. VI). The vertical lines indicate the limits of the fitted region.

Using the same parametrization as case 1 but only four parameters for the s wave instead of seven, we were able to obtain a solution (case 3) for which δ_0^0 lies outside the computed error bars in the region 650 to 850 MeV. It can therefore be considered a different solution quantitatively although the general variation of δ_0^0 with $\pi\pi$ mass is not very different. The other phase shifts have changed less than 1 standard deviation. The χ^2 for this fit is 173.0 for 150 degrees of freedom, which is somewhat worse than case 1 ($\chi^2 = 164.6$ for 147 degrees of freedom) but cannot be ruled out. In Table VIII we give δ_0^0 for this solution, and Fig. 14 contrasts it with δ_0^0 for case 1. This solution is of interest because it does not have an ϵ pole, and the phase shift is closer to the elastic down solution of Baton *et al.*[14] below 900 MeV. Even more than case 2, this solution indicates clearly that

TABLE VIII. Phase shifts for case 3.

$M_{\pi\pi}$ (GeV)	δ_0^0 (deg)	$M_{\pi\pi}$ (GeV)	δ_0^0 (deg)
0.55	47 ± 3	0.85	82 ± 5
0.625	54 ± 3	0.87	86 ± 5
0.665	58 ± 4	0.89	92 ± 5
0.69	61 ± 4	0.91	99 ± 5
0.71	63 ± 4	0.935	112 ± 6
0.73	65 ± 4	0.965	136 ± 7
0.745	67 ± 4	1.0	184 ± 9
0.755	68 ± 4	1.04	203 ± 9
0.765	69 ± 4	1.075	213 ± 9
0.775	70 ± 4	1.105	217 ± 9
0.785	71 ± 4	1.135	221 ± 9
0.795	73 ± 4	1.150	222 ± 9
0.810	75 ± 4		
0.83	78 ± 4		

our data are not sufficiently accurate to determine whether a broad ϵ exists. The S^* pole for this solution is at $996 - i52$ on the second sheet. The M-matrix parameters for cases 2 and 3 are given in Table IX.

How unique is our solution? We believe that the general features are unique: All the fits that we found with reasonable χ^2 gave very similar phase shifts and inelasticities in the fitted region. In particular, we feel that the evidence for the S^* pole is conclusive. An ϵ pole may be needed to explain the s-wave phase shift below 900 MeV, but without more accurate data (especially below 600 MeV) it is difficult to prove its existence. There is also some uncertainty concerning the inelasticities of the higher waves. In order to fit the moments we need substantial inelasticity in the d and f waves, much less in the p wave, although solutions with smaller η_1^1 than given by the selected fit could be obtained. Without more detailed information on the other channels one cannot choose among the various possibilities. In addition, the amount of inelasticity needed in these waves is inconsistent with the number of events observed in the 4π channels. A possible explanation is that above 1 GeV the moments obtained by a linear extrapolation tend to be systematically higher than the true physical moments, perhaps because of absorption effects (see Sec. VII B). Another possibility, although this seems less likely, is that the extrapolated $\omega\pi$ cross section is much larger than the one observed in $\pi^+ p \to \omega\pi^0\Delta^{++}$ and the small inelasticities actually reflect very strong couplings for the reaction $\pi^+\pi^- \to \omega\pi^0$. Because of this complication and the lack of clear structure in the moments beyond 1150 MeV, we do not feel that the extrapolated data are sufficiently sensitive to warrant extending the analysis beyond this point.

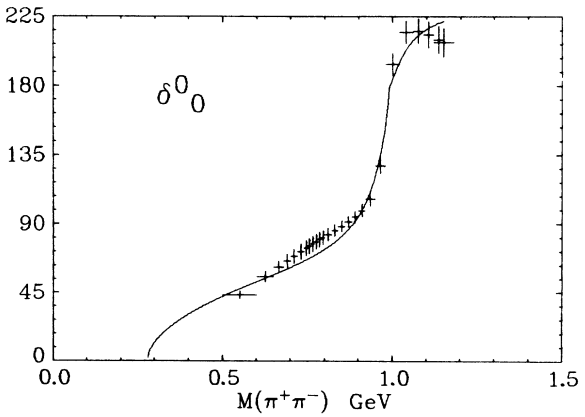

FIG. 14. The vertical lines give computed errors and the horizontal lines give the mass bins for the case-1 solution for δ_0^0. The solid line is the case-3 solution (four parameters for the $I=0$ s wave).

TABLE IX. M-matrix parameters for cases 2 and 3.[a]

Case	M_{11}^0	M_{12}^0	M_{22}^0	M_{11}^1	M_{12}^1	M_{22}^1	M_{12}^2
2	−0.358	2.14	−0.143	−0.68	2.61	−2.32	−0.186
3	3.38	2.40	0.071	0	0	−0.0038	0

[a]Units are in appropriate powers of $\mu(\pi$ mass).

VI. ENERGY-INDEPENDENT ANALYSIS

From the data and analysis presented in the previous sections it is clear that up to about 930 MeV, $\pi\pi$ scattering is dominated by only s and p waves. The small number of events in the 4π channels (Figs. 3 and 4) also indicate that one can assume those waves to be elastic up to 930 MeV, so an energy-independent analysis is relatively simple and straightforward. It is of interest then to do a point-by-point analysis and see how well one can eliminate ambiguities without imposing continuity.

In order to reduce the errors the mass bins used to extrapolate Y_L^0 moments and σ_{tot} are two times larger for this analysis than they are for the energy-dependent analysis (Fig. 10). Although a linear extrapolation for the cross section seems to work well, the need to include DP form factors makes the results somewhat model-dependent. On the other hand, $\langle Y_1^0\rangle$ and $\langle Y_2^0\rangle$ have a smooth linear dependence on t in the physical region, so the extrapolated values are likely to be more reliable. In addition, absorption-model calculations by Williams[33] indicate that for these moments linear extrapolation in t should be adequate (within 10%). Therefore, we will try to extract as much information as possible, using only the moments, and will point out explicitly when the cross-section information is used.

We define

$$\begin{aligned} s^2 &= \text{percentage of } s \text{ wave} \\ &= |S|^2 \frac{4\pi\lambda^2}{\sigma}, \\ p^2 &= \text{percentage of } p \text{ wave} \\ &= |P|^2 \frac{4\pi\lambda^2}{\sigma}, \end{aligned} \tag{6.1}$$

where S and P are the s- and p-wave amplitudes, respectively. Since we assume that only these waves are important, we have

$$\begin{aligned} \langle Y_1^0\rangle &= \left(\frac{1}{\pi}\right)^{1/2} sp\cos\alpha, \\ \langle Y_2^0\rangle &= \left(\frac{1}{5\pi}\right)^{1/2} p^2, \\ s^2 + p^2 &= 1, \\ \alpha &= \text{relative phase between } s \text{ and } p \text{ waves}. \end{aligned} \tag{6.2}$$

TABLE X. Energy-independent analysis: $\langle Y_1^0\rangle$, $\langle Y_2^0\rangle$, σ, p^2, s^2, and α.

Mass bin (GeV)	$\langle Y_1^0\rangle$	$\langle Y_2^0\rangle$	σ (mb)	p^2	s^2	α
0.50–0.60	0.164 ± 0.015	0.090 ± 0.015	18.9 ± 2.5	0.36 ± 0.06	0.64 ± 0.06	53 ± 4
0.55–0.63	0.164 ± 0.015	0.117 ± 0.015	23.5 ± 3.0	0.46 ± 0.06	0.54 ± 0.06	54 ± 4
0.60–0.65	0.170 ± 0.017	0.156 ± 0.016	40.2 ± 2.0	0.62 ± 0.06	0.38 ± 0.06	51 ± 5
0.63–0.68	0.187 ± 0.014	0.174 ± 0.013	56.2 ± 2.3	0.69 ± 0.05	0.30 ± 0.05	44 ± 5
0.65–0.70	0.195 ± 0.013	0.181 ± 0.012	61.2 ± 2.5	0.72 ± 0.05	0.28 ± 0.05	40 ± 6
0.68–0.72	0.191 ± 0.013	0.192 ± 0.012	78.9 ± 3.0	0.76 ± 0.05	0.24 ± 0.05	37 ± 7
0.70–0.74	0.195 ± 0.011	0.197 ± 0.010	104.2 ± 3.3	0.78 ± 0.04	0.22 ± 0.04	34 ± 7
0.72–0.75	0.202 ± 0.012	0.204 ± 0.011	122 ± 4.0	0.81 ± 0.04	0.19 ± 0.04	24 ± 13
0.74–0.76	0.188 ± 0.014	0.204 ± 0.012	133 ± 5.0	0.81 ± 0.05	0.19 ± 0.05	32 ± 11
0.75–0.77	0.153 ± 0.014	0.198 ± 0.012	134 ± 5.0	0.79 ± 0.05	0.21 ± 0.05	49 ± 6
0.77–0.79	0.196 ± 0.014	0.261 ± 0.013	121 ± 5.0	No solution		
0.79–0.83	0.185 ± 0.013	0.227 ± 0.011	113 ± 4.0	No solution		
0.82–0.86	0.186 ± 0.013	0.204 ± 0.012	75.2 ± 2.8	0.81 ± 0.05	0.19 ± 0.05	33 ± 10
0.84–0.88	0.180 ± 0.015	0.209 ± 0.014	58.9 ± 2.4	0.83 ± 0.06	0.17 ± 0.06	32 ± 14
0.86–0.90	0.165 ± 0.016	0.201 ± 0.015	49.5 ± 2.3	0.80 ± 0.06	0.20 ± 0.06	43 ± 9
0.88–0.92	0.158 ± 0.017	0.196 ± 0.016	41.3 ± 2.1	0.78 ± 0.06	0.22 ± 0.06	47 ± 8
0.90–0.96	0.174 ± 0.015	0.171 ± 0.015	35.2 ± 1.5	0.68 ± 0.06	0.32 ± 0.06	48 ± 5

From the above equations we can determine s^2, p^2, and α. The results are given in Table X.

Next we want to determine the phase shifts ($I=1$ p wave, δ_1^1; $I=0$ s wave, δ_0^0) for which we need the cross section. Clearly, since the p wave dominates we can obtain reasonable values for δ_1^1 by using the relation $\sigma_p \equiv p^2\sigma = 12\pi\lambda^2 \sin\delta_1^1$, which determines δ_1^1 (modulo $\frac{1}{2}\pi$, but the ambiguity in this case is trivial). We should note that if δ_1^1 is changed by more than 1 standard deviation from the value obtained with the cross section, usually no solutions can be found for δ_0^0. We define now

$$\delta_s = \delta_1^1 \pm \alpha. \tag{6.3}$$

If the $I=2$ s-wave phase shift (δ_0^2) is 0°, then $\delta_s = \delta_0^0$. One obtains then two values for δ_0^0, but note that this ambiguity is different from the one obtained solving for

$$\frac{\sigma}{4\pi\lambda^2}\langle Y_1^0\rangle = 3\left(\frac{1}{\pi}\right)^{1/2} \sin\delta_0^0 \sin\delta_1^1 \cos(\delta_1^1 - \delta_0^0)$$

(assuming $\delta_0^2 = 0$), (6.4)

where the equation is also satisfied for $\delta_0^{0\prime} = \frac{1}{2}\pi + (\delta_1^1 - \delta_0^0)$. This is the usual up-down ambiguity

TABLE XI. Energy-independent analysis: δ_1^1, $(\delta_0^0)^1$, $(\delta_0^0)^2$, s_1^2, s_2^2, σ_s^1, and σ_s^2.

Mass bin (GeV)	δ_1^1 (deg)	1 st solution $s^{2\,a}$	σ_s (mb)	δ_0^0 (deg)	1 st solution $s^{2\,b}$	σ_s (mb)	2nd solution δ_0^0 (deg)	2nd solution $s^{2\,b}$	2nd solution σ_s (mb)
0.50–0.60	9.2 ± 2.0	0.64 ± 0.06	12 ± 2	58 ± 5	0.78 ± 0.05	26 ± 3	134 ± 5	0.77 ± 0.05	22 ± 4
0.55–0.63	13 ± 2	0.54 ± 0.06	13 ± 2	63 ± 6	0.69 ± 0.05	25 ± 2	136 ± 6	0.62 ± 0.06	18 ± 3
0.60–0.65	21 ± 3	0.38 ± 0.06	15 ± 3	69 ± 6	0.48 ± 0.05	23 ± 3	147 ± 5	0.29 ± 0.06	10 ± 3
0.63–0.68	29 ± 3	0.31 ± 0.05	17 ± 3	68 ± 6	0.35 ± 0.04	21 ± 2	163 ± 6	0.08 ± 0.04	3 ± 2
0.65–0.70	32 ± 3	0.28 ± 0.05	17 ± 3	67 ± 6	0.30 ± 0.04	19 ± 2	174 ± 6	0.02 ± 0.02	1 ± 1
0.68–0.72	40 ± 4	0.24 ± 0.05	19 ± 4	72 ± 8	0.24 ± 0.02	19 ± 2	...	...	...
0.72–0.75	62 ± 7	0.19 ± 0.04	23 ± 5	80 ± 15	0.16 ± 0.02	19 ± 2	29 ± 15	0.03 ± 0.03	3 ± 3
0.74–0.76	70 ± 11	0.19 ± 0.05	25 ± 7	97 ± 16	0.15 ± 0.02	17 ± 3	28 ± 16	0.03 ± 0.03	3 ± 2
0.75–0.77	72 ± 12	0.21 ± 0.05	29 ± 7	114 ± 14	0.14 ± 0.04	17 ± 5	...	...	...
0.77–0.83	...	...	...	...	...	...	...	...	...
0.82–0.86	126 ± 5	0.19 ± 0.05	14 ± 4	86 ± 11	0.20 ± 0.02	15 ± 3	158 ± 11	0.06 ± 0.04	4 ± 3
0.84–0.88	132 ± 5	0.17 ± 0.05	10 ± 3	92 ± 15	0.23 ± 0.03	15 ± 2	165 ± 15	0.04 ± 0.04	2 ± 2
0.96–0.90	137 ± 5	0.20 ± 0.06	10 ± 3	85 ± 10	0.26 ± 0.03	14 ± 2	180 ± 10	0 ± 0.01	0 ± 2
0.88–0.92	141 ± 5	0.22 ± 0.06	9 ± 3	84 ± 9	0.29 ± 0.02	13 ± 1	...	...	...
0.90–0.96	146 ± 4	0.32 ± 0.06	11 ± 2	88 ± 6	0.34 ± 0.02	12 ± 1	...	...	...

[a] s^2 obtained from Eq. (6.2).
[b] s^2 obtained from Eqs. (6.7) and (6.8).

TABLE XII. Comparison of experimental moments with those computed from "up" and "down" solutions.

	Energy-independent solution					$\delta_0^{0\prime}=\frac{1}{2}\pi-\delta_0^0+\delta_1^1$				Energy-dependent solution				
$M_{\pi\pi}$ (GeV)	δ_1^1 (deg)	δ_0^0 (deg)	$\Delta Y_2^{0\,a}$	$\Delta Y_2^{0\,a}$	$\sqrt{\chi^2}$ [b]	$\delta_0^{0\prime}$ (deg)	$\Delta Y_1^{0\,a}$	$\Delta Y_2^{0\,a}$	$\sqrt{\chi^2}$ [b]	δ_1^1 (deg)	δ_0^0 (deg)	$\Delta Y_1^{0\,a}$	$\Delta Y_2^{0\,a}$	$\sqrt{\chi^2}$
0.50–0.60	9.2± 2	58± 5	1.7	2.6	3.1	41± 5	−3.2	0.7	3.3	9.8± 7	44± 2	−1.9	1.4	2.4
0.55–0.62	12.9± 2.3	63± 4	0.82	2.6	2.7	40± 5	−5.1	−0.4	5.1	13.8± 1.0	51± 3	−2.4	1.1	2.6
0.60–0.65	21.4± 2.6	68± 5	−0.3	1.6	1.66	43± 5	−3.8	−1.1	4.0	20.2± 1.0	57± 3	−1.8	1.5	2.3
0.63–0.68	28.8± 2.7	68± 6	−0.4	0.74	0.8	50± 6	−2.3	−1.0	2.5	27.1± 1.0	63± 4	−0.79	0.95	1.2
0.65–0.70	32± 3	67± 6.4	−0.28	0.36	0.5	55± 7	−1.4	−0.7	1.6	33.0± 1.0	66± 4	−0.05	0.17	0.18
0.68–0.72	40.5± 3.5	73± 8	−0.03	0.014	0.04	58± 8	−1.02	−1.05	1.5	43.9± 1.0	70± 4	−0.16	−0.54	0.56
0.70–0.74	51.3± 4.3	79± 8	0.85	−0.72	1.1	62± 8	0.03	−1.7	1.7	54.2± 1.5	72.5± 4	0.3	−1.2	1.3
0.72–0.75	62± 6	80± 12	1.15	−0.76	1.4	71± 12	0.90	−1.08	1.4	64.8± 1.5	74.5± 4	1.0	−1.0	1.4
0.74–0.76	70.2± 7	97± 15	1.2	−0.85	1.5	63± 16	0.67	−1.63	1.8	75.3± 1.6	76.4± 4	−0.03	−1.2	1.2
0.75–0.77	71± 7	115± 14	1.82	−1.68	2.48	46± 15	1.13	−3.0	3.3	81.1± 1.6	77.3± 4	−2.4	−1.8	3.0
0.82–0.86	126± 5	86± 10	−0.14	−0.09	0.2	130± 10	−0.97	−0.92	1.3	126± 1.2	85± 4	0.39	0.10	0.4
0.84–0.88	132± 5	93± 10	−1.4	1.09	1.8	129± 11	−2.3	0.13	2.3	133± 1.1	87± 4	0.09	1.1	1.1
0.86–0.90	137± 5	85± 9	−0.86	0.87	1.2	142± 10	−2.33	−0.80	2.5	138± 1.0	89± 4	−0.76	1.2	1.4
0.88–0.92	141± 5	84± 9	−0.86	1.04	1.3	146± 10	−2.7	−0.98	2.9	143± 1.0	94± 4	−1.1	1.6	1.9
0.90–0.96	145± 4	88± 6	−0.22	0.41	0.5	147± 6	−3.0	−2.2	3.7	149± 1.0	104± 5	−0.97	1.6	1.9

[a] $\Delta Y_L^0 \equiv (\langle Y_L^0\rangle_{\rm calc} - \langle Y_L^0\rangle_{\rm exp})/\sigma_{\rm exp}$.

[b] $\sqrt{\chi^2} \equiv [(\Delta Y_1^0)^2 + (\Delta Y_2^0)^2]^{1/2}$.

pointed out by Gutay *et al.*,[34] which we will discuss later on.

We now compute δ_0^0 from the two values of δ_s. It is trivial to show that

$$\tan\delta_s = \frac{\frac{2}{3}\sin^2\delta_0^0 + \frac{1}{3}\sin^2\delta_0^2}{\frac{2}{3}\cos\delta_0^0\sin\delta_0^0 + \frac{1}{3}\cos\delta_0^2\sin\delta_0^2}\ , \tag{6.5}$$

from which follows, after some algebra,

$$\tan\delta_0^0 = \{\tfrac{1}{2}\tan\delta_s \pm [\tfrac{1}{4}\tan^2\delta_s - \beta(1+\beta)]^{1/2}\}/(1+\beta)\ , \tag{6.6}$$

where

$$\beta = \tfrac{1}{2}(\sin^2\delta_0^2 - \sin\delta_0^2\tan\delta_s)$$

and the sign should be chosen such that $\tan\delta_0^0 = \tan\delta_s$ when $\delta_0^2 = 0$. Note that Eq. (6.6) may not have a solution if $\tan^2\delta_s < 4\beta(1+\beta)$; this indeed happens at some energies for one of the two possible solutions. For δ_0^2 we use the same phase shifts as in Sec. IV. The effect of δ_0^2 is small, and even large errors on δ_0^2 will change δ_0^0 by very little. We define

$$\sigma_s \equiv s^2\sigma$$

$$= 4\pi\lambda^2[\tfrac{4}{9}\sin^2\delta_0^0 + \tfrac{4}{9}\sin\delta_0^0\sin\delta_0^2\cos(\delta_0^0-\delta_0^2) + \tfrac{1}{9}\sin^2\delta_0^2]. \tag{6.7}$$

Clearly,

$$s^2 = \sigma_s/(\sigma_s+\sigma_p)\ . \tag{6.8}$$

We now compute s^2 and σ_s from our phase shifts (δ_0^0 and δ_1^1), and compare them to the ones obtained directly from the Y_2^0 moment and the cross section. This will tell us if one solution can be favored over the other and whether our extrapolated cross section is consistent with the extrapolated moments. The results are tabulated in Table XI. Excepting for the two points below 600 MeV, it is quite apparent that one of the two solutions at each energy is in very good agreement with s^2 and p^2 computed directly, while the other is not. No solution can be obtained between 770 and 820 MeV; the Y_1^0 and Y_2^0 moments are inconsistent with each other, giving either $p^2>1$ or $\cos\alpha>1$. We believe that the main reason is ρ-ω interference, which we shall discuss in more detail in Sec. VII. It is clear that the ambiguity given by Eq. (6.3) is easily resolved, at least above 600 MeV. Can we resolve the usual up-down ambiguity? With our values for δ_1^1 and δ_0^0 we can compute $\delta_0^{0\prime} = \frac{1}{2}\pi - \delta_0^0 + \delta_1^1$ and recompute $\langle Y_1^0\rangle$ and $\langle Y_2^0\rangle$ with the new δ_0^0 phase shift. We could try to distinguish between the two by using the cross section, but this depends on how well we know our normalization and on the reliability of using DP form factors. We will therefore limit ourselves to the moments. In Table XII we give how many standard deviations $\langle Y_1^0\rangle$ and

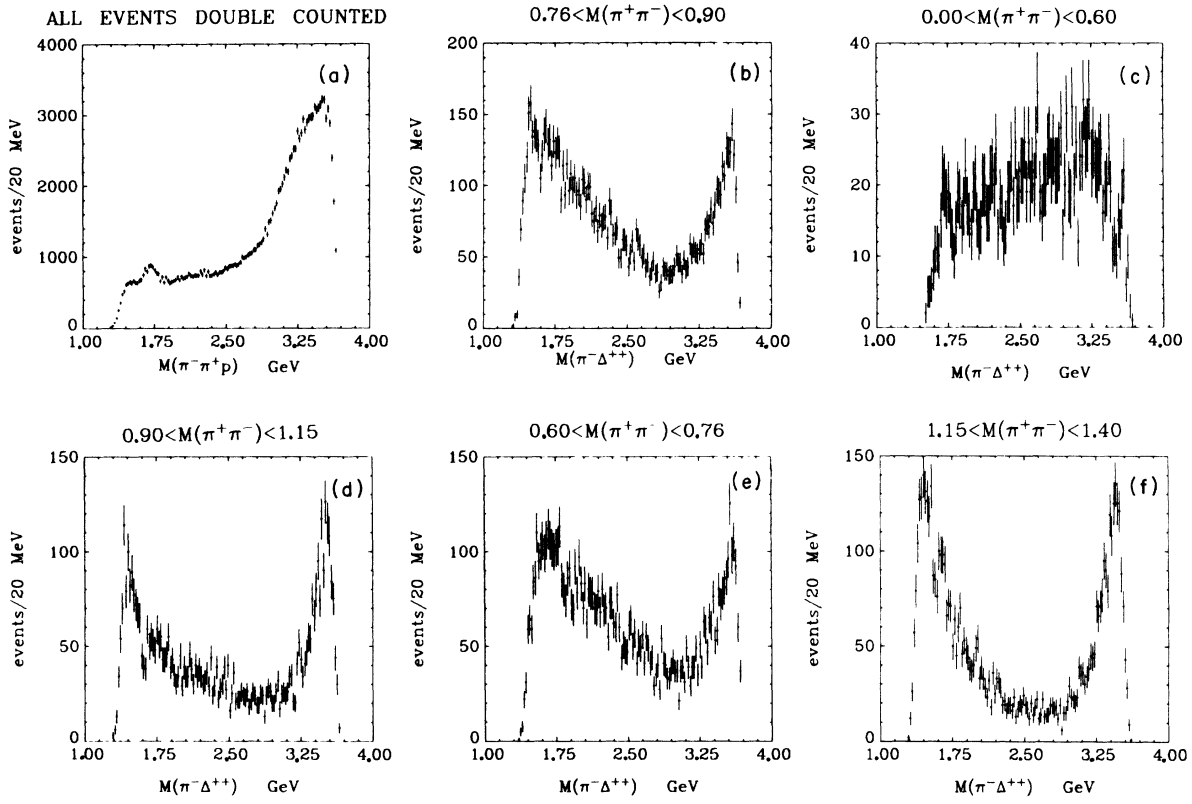

FIG. 15. Mass distributions of π-Δ^{++} event for reaction $\pi^+p \to \pi^+\pi^-\Delta^{++}$ and various $\pi^+\pi^-$ mass cuts; with $|t_{p\Delta}|<0.4$ GeV^2, except for (a) which contains all the events.

$\langle Y_2^0 \rangle$ (computed from the phase shifts) are from the extrapolated values, both for the energy-independent and energy-dependent solutions. Clearly, between 700 and 880 MeV, one cannot separate the two ambiguous solutions on a point-by-point basis by using only the moments. Between 900 and 960 MeV the "up" solution ($\delta_0^0 \approx 140°$) is 3.7 standard deviations away from the extrapolated moments; a value for δ_0^0 closer to 90° seems to be strongly favored. However, we must point out that because of the uncertainties in extrapolation procedures, the separation between the two solution should be considered less significant than what the errors indicate.

With the energy-independent analysis we can reach the firm conclusion that δ_0^0 is between 60° and 70° near 700 MeV, in agreement with the unique results of Baton *et al.*[14] and Baillon *et al.*[27] The structure in our data in the region between 950 and 1000 MeV indicates without doubt that the s wave is varying rapidly in that region. In particular, the rapid drop in the cross section between 950 and 980 MeV indicates that the s-wave amplitude must be large (i.e., $\delta_0^0 \approx 90°$) before 950 MeV.[3] It is this observation that permits us to obtain a unique solution for δ_0^0. With our energy-dependent analysis we have found a parametrization for the s wave that connects smoothly the unique values below 700 MeV with those above 950 MeV. Barring any fine structure, it is unlikely that a continuous solution would go through points corresponding to the "up" solution between 780 and 900 MeV. Note from Fig. 11 that the "up" and "down" solutions are well separated. For the "up" branch to join the observed value at 900 MeV, δ_0^0 would have to decrease by about 40° within 20 MeV. From the Wigner condition of causality,[35] $d\delta/dq > -R$, this would imply a radius of interaction of at least 15 F, which is unreasonable. The other possibility is that the phase shift goes through 180° before 900 MeV, implying that $\langle Y_1^0 \rangle$ is zero somewhere in that region, which is certainly not the case within our resolution (±5 MeV in the ρ region). We feel therefore that our energy-dependent solution for δ_0^0 gives the correct qualitative behavior of the s-wave amplitudes as a function of $\pi\pi$ mass. The actual quantitative values may have systematic deviations because of the effects non-π-exchange background and absorption have on the extrapolation.

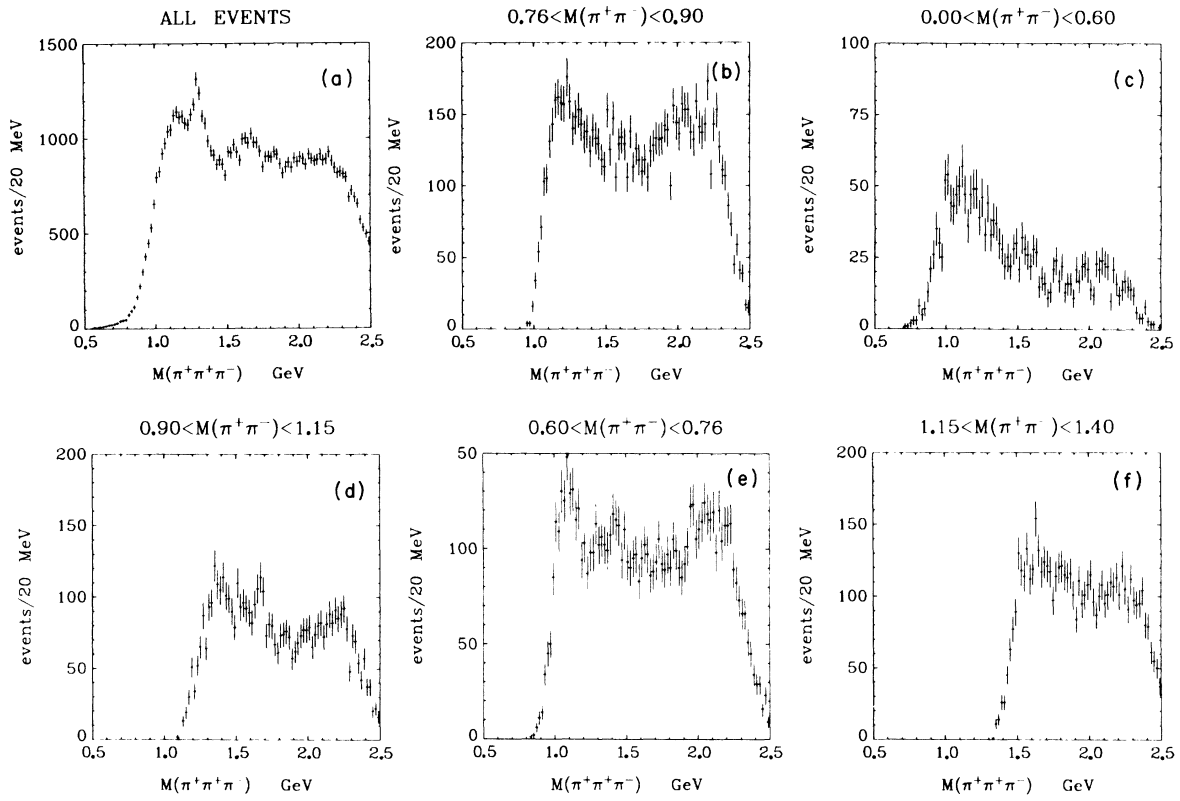

FIG. 16. Mass distributions of $\pi^+\pi^+\pi^-$ events for reaction $\pi^+p \to \pi^+\pi^-\Delta^{++}$ and various $\pi^+\pi^-$ mass cuts, with $|t_{p\Delta}| < 0.4$ GeV^2, except for (a) which contains all the events.

VII. SOURCES OF UNCERTAINTY IN THE EXTRAPOLATION TO THE π POLE

A. Three-Body Resonances

Although in principle extrapolating to the π pole should eliminate the background contribution of $\pi^+\pi^-p$ and $\pi^+\pi^+\pi^-$ resonances, in practice significant three-body resonance production is likely to affect the results because of finite statistics. In Figs. 15 and 16 we show the $\pi^+\pi^-p$ and $\pi^+\pi^+\pi^-$ mass distributions for all the events and with various cuts in $\pi^+\pi^-$ mass for the events used in the extrapolation. When all the events are considered there are clear A_1, A_2, and A_3 signals in the $\pi^+\pi^+\pi^-$ systems, and also a strong $N^*(1680)$ signal in $\pi^+\pi^-p$ and some indications of lower-mass N^*'s. But once events with a Δ^{++} and $|t_{p\Delta}| < 0.4$ GeV^2 are selected, the A_2 and $N^*(1680)$ signals disappear for all $\pi^+\pi^-$ masses up to 1.4 GeV. How much of the enhancements (especially at low mass) is due to three-body resonances (or diffraction) and how much to reflections of the $\pi^+\pi^-$ system (or π^+p system) is probably impossible to ascertain without a detailed production model. To establish such a model, data at many different incident beam momenta are required. However, there is no obvious three-body resonance production that would contribute significantly to non-π-exchange background. The most noticeable candidate for a three-body resonance is in Fig. 16(d) around 1600 MeV, which could at most contribute a 2% background.

B. Absorption Effects

Many years ago Gottfried and Jackson pointed out that initial- and final-state interactions should modify the one-pion-exchange model.[36] Essentially, instead of the simple diagram in Fig. 17(a),

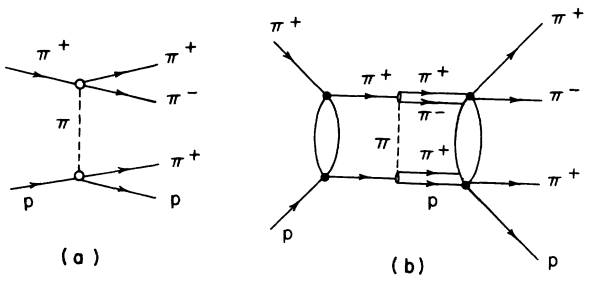

FIG. 17. (a) One-pion-exchange diagram. (b) One-pion-exchange diagram with absorption.

TABLE XIII. Phases (in degrees) and inelasticities after modifying higher moments.

Mass (GeV)	δ_0^0	η_0^0	δ_1^1	η_1^1	δ_2^0	η_2^0	δ_3^1	η_3^1
0.91	97± 4		145± 8		3.8± 1		−1.3± 0.5	0.96± 0.02
0.935	106± 5		149± 9	0.99± 0.01	5.5± 1		−1.2± 0.6	0.89± 0.05
0.965	128± 6		152± 1	0.99± 0.01	7.8± 1.2	0.99± 0.01	−1.0± 0.7	0.85± 0.05
1.0	196± 9	0.37± 0.08	155± 1.2	0.99± 0.01	11± 1.4	0.93± 0.03	−0.6± 0.8	0.84± 0.05
1.04	224± 0	0.38± 0.04	157± 1.6	0.97± 0.03	17± 2	0.80± 0.06	0± 0.7	0.85± 0.05
1.075	226± 8	0.45± 0.04	159± 2.5	0.97± 0.05	25± 3	0.72± 0.08	1± 0.8	0.87± 0.05
1.105	223± 8	0.50± 0.04	159± 3.4	0.95± 0.06	32± 4	0.75± 0.06	2± 1.1	0.90± 0.06
1.135	220± 8	0.55± 0.04	159± 4	0.91± 0.06	37± 5	0.86± 0.04	4± 1.8	0.94± 0.07
1.150	217± 7	0.60± 0.04	158± 6	0.88± 0.07	42± 7	0.90± 0.04	4.5± 2.0	0.95± 0.10

one should consider the diagram of Fig. 17(b). Because the lower partial waves of the initial π^+p system (or final $\rho\Delta^{++}$ system) have higher probability of contributing to other channels, these waves are said to be absorbed. This is an alternative explanation to Dürr-Pilkuhn form factors for the fact that the $t_{p\Delta}$ distribution is more sharply peaked in the forward direction than what one would expect from a naive one-pion-exchange model.

Williams has done model calculations which show how absorption may modify the simple linear extrapolations of Y_L^0 moments.[33] His calculations indicate that a linear extrapolation of the Y_1^0, Y_2^0, and Y_3^0 moments may miss the true value at the π pole by 10% or less, which is within our errors. However, the Y_4^0 moment has a rapid turnover in the unphysical region, and a linear extrapolation is likely to overestimate the value at the π pole by 25% or more. Although he has not done the calculation for the higher moments, the same kind of effect is probably to be expected. We have therefore re-done our fit assuming that the $\langle Y_L^0\rangle$ ($L \geq 4$) are 30% smaller than those used in Sec. VI. These corrections only affect the phase shifts above 900 MeV. The χ^2 for this fit is 133.2 for 147 degrees of freedom. In Table XIII we show the new phase shifts and in Table XIV the new M-matrix parameters. We must emphasize that the corrections are quite uncertain and model-dependent. The main effect is to give more reasonable d and f waves. In particular the f wave is much less inelastic, although the inelasticity is still a bit too small to be consistent with other channels. The s-wave phase shift is now somewhat larger above 1.0 GeV. The ϵ pole is hardly affected, being at $656 - i328$ MeV (II sheet), while the S^* has become narrower, $998 - i20$ MeV. Computed errors are of the same size as previously quoted. See Appendix A, Table XV, for the effect of absorption corrections on the case-3 fit.

C. Effect of ρ-ω Interference

As indicated in Sec. VI, the extrapolated cross section has a dip and $\langle Y_2^0\rangle$ a spike not predicted by our fit, in the region 760 to 800 MeV. In Fig. 18 we show the mass distribution and $N\langle Y_2^0\rangle$ vs $\pi\pi$ mass for various t' cuts. We chose to plot $N\langle Y_2^0\rangle$ in this case because it depends only on the p-wave amplitude (assuming higher waves give a negligible contribution) and shows clearly that the effect near the ω mass is indeed a p-wave effect. It would be beyond the scope of this article to discuss ρ-ω interference in detail. One needs to determine first the production amplitude for the reaction $\pi^+p \to \Delta^{++}\omega$ at a given beam momentum and use that as an input to the reaction $\pi^+p \to \pi^+\pi^-\Delta^{++}$ at the same momentum. That will be the subject of a future article. We will limit ourselves to discussing why the extrapolation to the π pole is unable to remove the effect.

Ratcliff *et al.*[37] have observed a striking effect in the reaction $\pi^-p \to \pi^+\pi^-n$ at 15 GeV/c near the ω mass for $0.1 < |t| < 0.3$ GeV^2, which is not visible for $|t| < 0.1$ GeV^2. They also show that the ω must be produced mostly with $m = \pm 1$. If this were the case for our reaction no trace of ρ-ω interference should be present in our extrapolated data. It is evident from Fig. 18 that in our case an effect is noticeable only at small t', for $|t'| < 0.03$ GeV^2 and $0.03 < |t'| < 0.1$ GeV^2, while it is not significant for $0.1 < |t'| < 0.3$ GeV^2. This indicates that the ω must be produced with significant amounts of $m = 0$ com-

TABLE XIV. M-matrix parameters after modifying higher moments.

$M_{11}^0 = -0.99 \pm 2.2$	$M_{12}^0 = 1.87 \pm 0.45$	$M_{22}^0 = 0.032 \pm 0.4$
$M_{11}^1 = -0.087 \pm 0.70$	$M_{12}^1 = 0.212 \pm 0.67$	$M_{22}^1 = -0.31 \pm 0.50$
	$M_{12}^2 = 0.0030 \pm 0.0007$	

TABLE XV. M-matrix elements and pole structure for various fits in restricted mass intervals.[a]

Mass interval (GeV)	No. of points	χ^2	Poles	M^0_{11}	M^0_{12}	M^1_{11}	M^1_{12}	M^1_{22}	M^0_{22}	No. of variable parameters
0.935–1.04	33	32.5	II (1002, 33)	2.30	1.96	0	0	0	−0.024	3
0.935–1.04	33	35.7	II, IV (976, 52), (974, 50)	−0.022	1.99	0	0.181	0	0.02 (fixed)	3
0.935–1.04	33	31.5	II (1005, 31)	1.39	2.02	0	0	−0.0706	0.02 (fixed)	3
0.935–1.1	47	46.3	II, IV (974, 37), (1001, 49)	−0.097	1.73	0	0.176	0	−0.028	4
0.935–1.1	47	36.1	II (1007, 30)	1.35	2.05	0	0	−0.077	−0.064	4
0.55–1.15	171	143.3	II (993, 43)	3.03	2.16	0	0	−0.0054	−0.028	21 4 for s wave

[a] All fits except number 6 keep the parameters of $L \neq 0$ waves fixed at the values obtained for our case 1 fit.

ponents in the reaction $\pi^+ p \to \omega \Delta^{++}$ at 7.1 GeV/c (especially at small t), which is consistent with preliminary studies of that reaction.

In conclusion then, because ρ-ω interference in our case seems to be most significant at small t, the extrapolation to the π pole tends to enhance the effect instead of removing it as one would normally expect. A possible explanation for the enhancement of the effect at low t being as rapid as anything produced by π exchange – and we emphasize that this is only a speculation at this point point – is that the $m = \pm 1$ and $m = 0$ amplitudes interfere with nearly opposite signs, canceling each other when they are of comparable magnitude, but at small t the $m = \pm 1$ amplitudes vanish rapidly while the $m = 0$ ω amplitude is still appreciable.

VIII. CONCLUSIONS

A coupled-channel analysis ($\pi\pi$ and $K\bar{K}$) with a 2×2 M matrix has yielded fruitful results on the $I = 0$ $\pi\pi \to \pi\pi$ s-wave scattering amplitude. The very marked structure of our data puts sufficient constraints to eliminate the "up-down" ambiguity, leaving the "down" solution as the only viable one between 550 and 950 MeV. There are still quantitative uncertainties, in particular regarding how close to 90° the $I = 0$ s-wave phase shift (δ^0_0) may be in the ρ region, but the possibility of a narrow ϵ resonance is definitely ruled out by our solutions. Searching for poles in the complex energy plane, we found two of interest. One (S^*) is very close to the $K\bar{K}$ threshold on the second Riemann sheet, at $997 \pm 6 - i(27 \pm 8)$. The other (ϵ) is far from the physical region, at $660 \pm 100 - i(320 \pm 70)$ MeV on the second Riemann sheet. The S^* pole was present in all the fits we obtained with reasonable χ^2, and we feel the evidence for its existence is conclusive. Whether one could find an ϵ on the second sheet depended on parametrization, and it is clear that much more accurate data are needed to either rule it out or prove it exists. In addition the 4π cut, which we neglect, might have to be taken into account. We feel our solutions are qualitatively correct, but the actual quantitative values may have systematic deviations because of uncertainties in the extrapolation. The actual mass and width of the ρ resonance are probably affected by ρ-ω interference, while the d and f waves are likely to be modified because of absorption corrections. Unfortunately, all these corrections are model-dependent and a solid, reliable production model is needed before one can take them into account properly.

ACKNOWLEDGMENTS

We thank Professor G. F. Chew, Dr. G. Smadja, Dr. M. R. Pennington, and Dr. E. Colton for many useful discussions. We thank Joseph J. Murray for his work in beam design and construction, the Stanford Linear Accelerator 82-in. Bubble Chamber Group for their assistance in data gathering, and the LBL Group A Scanning and Measuring Group for their help in data reduction.

APPENDIX A

With our M-matrix parametrization for the $I = 0$ s wave, we find in addition to the second-sheet pole (997, 27) a third-sheet pole at (930, 18) which can be said to be just as close to the physical region.[38] This pole is present in both case-1 and case-2 fits. More than one pole in that region was also found in fits done to our previously published unextrapolated data by Kato and Fujii[39] with a quite different parametrization.

When more than one channel is taken into account and one finds a pole, one can expect by analytic continuation of the S matrix to find additional poles ("shadow" poles) on other unphysical sheets.[40] Is it then possible to unambiguously assign one pole

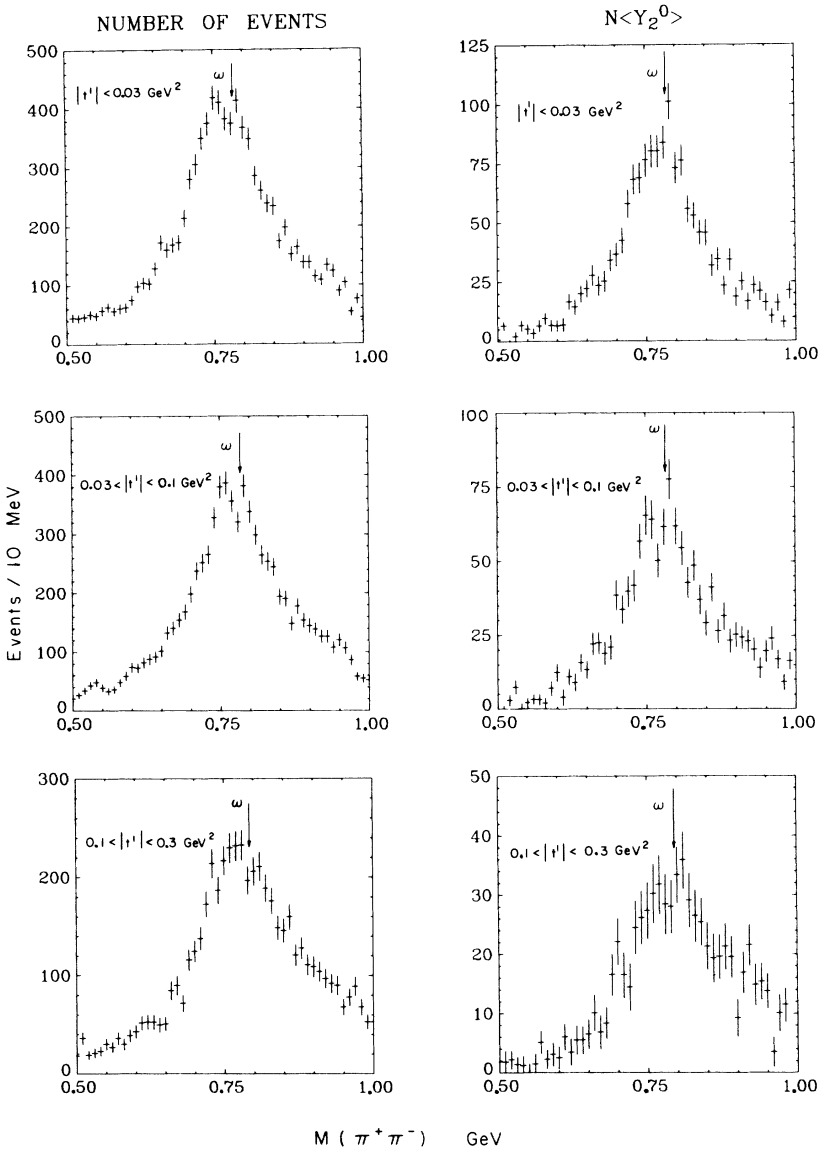

FIG. 18. $\pi^+\pi^-$ mass distributions and $N\langle Y_2^0\rangle$ in 10-MeV bins for various t' cuts. The arrow indicates the ω mass (783 MeV).

to an observed resonance? Usually the other poles are far from the physical region and only the nearest one can be said to be well determined from the data. But when the pole is very close to a threshold, as is the case for the S^*, "shadow" poles may be just as close and it is no longer clear whether a single pole is sufficient to describe the observed phenomena. In particular, it becomes problematical what values for the mass and width should be used for comparison with other members of an SU(3) multiplet. In our case the third-sheet pole residues R_{11} and R_{12} (see Table VII for definition) are half as big as for the second pole, while R_{22} is comparable. To determine whether the two

TABLE XVI. $K\bar{K}$ cross section.

Mass bin (GeV)	$\sigma_{K\bar{K}}$ (mb)
0.988–1.02	3.78± 0.53
1.02–1.06	2.90± 0.40
1.06–1.10	3.55± 0.47
1.10–1.14	2.80± 0.40
1.14–1.18	2.22± 0.37
1.18–1.22	2.41± 0.39
1.22–1.26	2.66± 0.41
1.26–1.30	4.4 ± 0.52
1.30–1.34	2.85± 0.42
1.36–1.40	2.85± 0.42

TABLE XVII. Extrapolated cross section and moments ($L = 1 - 6$).

Mass bin (GeV)	$\sigma_{\pi\pi}$ (mb)	$\langle Y_1^0 \rangle$	$\langle Y_2^0 \rangle$	$\langle Y_3^0 \rangle$	$\langle Y_4^0 \rangle$	$\langle Y_5^0 \rangle$	$\langle Y_6^0 \rangle$
0.28–0.49	6.5± 2.3	0.076± 0.015	0.076± 0.015	0.000± 0.015	0.008± 0.015	0.006± 0.015	0.006± 0.015
0.45–0.55	15.8± 2.6	0.149± 0.016	0.041± 0.016	0.007± 0.016	−0.013± 0.017	−0.002± 0.017	−0.005± 0.016
0.50–0.60	18.9± 2.5	0.164± 0.015	0.090± 0.015	−0.008± 0.016	−0.038± 0.016	−0.019± 0.016	−0.017± 0.016
0.60–0.65	40.3± 2.8	0.170± 0.017	0.156± 0.016	−0.009± 0.017	−0.015± 0.017	−0.011± 0.017	−0.016± 0.017
0.65–0.68	60.7± 3.1	0.203± 0.017	0.167± 0.016	0.013± 0.017	−0.021± 0.017	0.010± 0.017	0.001± 0.017
0.68–0.70	62.2± 3.9	0.187± 0.020	0.202± 0.018	−0.002± 0.012	0.018± 0.020	0.009± 0.02	0.020± 0.020
0.70–0.72	94.0± 4.5	0.199± 0.017	0.189± 0.015	0.031± 0.017	−0.010± 0.016	0.009± 0.016	0.002± 0.016
0.72–0.74	113.5± 4.9	0.191± 0.015	0.203± 0.013	0.008± 0.015	−0.004± 0.015	0.010± 0.015	0.003± 0.015
0.74–0.75	132.8± 7.3	0.224± 0.019	0.225± 0.017	0.011± 0.020	−0.003± 0.021	0.021± 0.021	−0.007± 0.021
0.75–0.76	132.3± 7.4	0.152± 0.020	0.180± 0.017	−0.027± 0.020	−0.021± 0.021	−0.016± 0.020	−0.028± 0.020
0.76–0.77	128.3± 7.5	0.153± 0.020	0.216± 0.017	−0.019± 0.020	−0.005± 0.020	0.000± 0.020	0.017± 0.019
0.77–0.78	108.2± 6.1	0.207± 0.021	0.261± 0.019	−0.013± 0.020	0.036± 0.022	0.010± 0.022	0.022± 0.022
0.78–0.79	125.5± 6.6	0.200± 0.020	0.273± 0.018	0.015± 0.021	0.020± 0.020	0.007± 0.020	0.009± 0.020
0.79–0.80	123.8± 7.1	0.171± 0.020	0.234± 0.018	0.009± 0.022	0.020± 0.022	−0.008± 0.022	−0.006± 0.022
0.80–0.82	104.7± 4.5	0.199± 0.016	0.234± 0.014	0.000± 0.016	−0.007± 0.016	−0.005± 0.017	0.009± 0.017
0.82–0.84	81.4± 4.1	0.189± 0.018	0.207± 0.015	0.028± 0.018	0.002± 0.017	0.014± 0.017	−0.001± 0.017
0.84–0.86	65.7± 3.6	0.186± 0.020	0.212± 0.018	0.043± 0.021	0.001± 0.021	0.013± 0.020	0.001± 0.025
0.86–0.88	58.3± 3.3	0.174± 0.024	0.204± 0.022	0.014± 0.025	0.004± 0.025	−0.008± 0.025	−0.011± 0.025
0.88–0.90	46.3± 3.1	0.160± 0.022	0.195± 0.021	−0.007± 0.025	0.024± 0.024	0.030± 0.024	0.018± 0.024
0.90–0.92	35.8± 2.8	0.157± 0.026	0.199± 0.024	0.027± 0.027	0.021± 0.026	0.010± 0.026	0.001± 0.027
0.92–0.95	34.2± 2.2	0.195± 0.022	0.166± 0.021	0.000± 0.024	0.033± 0.023	0.010± 0.023	0.031± 0.023
0.93–0.98	23.8± 2.0	0.175± 0.024	0.200± 0.025	−0.010± 0.026	0.065± 0.026	0.038± 0.026	0.006± 0.026
0.98–1.02	13.6± 1.3	0.036± 0.033	0.325± 0.026	−0.020± 0.033	0.076± 0.032	0.041± 0.033	0.039± 0.032
1.02–1.06	14.3± 1.3	−0.029± 0.034	0.271± 0.026	0.005± 0.032	0.085± 0.032	0.047± 0.032	0.018± 0.032
1.06–1.09	17.6± 1.6	0.017± 0.040	0.305± 0.031	0.017± 0.037	0.092± 0.036	0.044± 0.037	0.036± 0.037
1.09–1.12	15.8± 1.6	0.010± 0.041	0.298± 0.033	0.055± 0.042	0.124± 0.039	0.090± 0.040	0.043± 0.039
1.12–1.15	19.0± 1.7	−0.024± 0.042	0.326± 0.035	0.014± 0.042	0.111± 0.041	0.064± 0.042	0.024± 0.044
1.12–1.17	19.3± 1.2	0.035± 0.03	0.267± 0.024	0.017± 0.030	0.100± 0.029	0.077± 0.029	0.004± 0.030
1.15–1.20	21.9± 1.3	0.075± 0.032	0.265± 0.025	0.027± 0.031	0.087± 0.031	0.048± 0.031	0.003± 0.030
1.18–1.22	24.2± 1.6	0.092± 0.035	0.332± 0.027	0.056± 0.036	0.152± 0.034	0.079± 0.036	−0.005± 0.030
1.20–1.24	26.4± 1.8	0.084± 0.033	0.314± 0.026	0.055± 0.033	0.109± 0.031	0.084± 0.032	−0.091± 0.031
1.22–1.26	28.3± 1.9	0.077± 0.034	0.353± 0.026	0.117± 0.034	0.152± 0.031	0.129± 0.032	−0.054± 0.032
1.24–1.28	30.4± 2.0	0.084± 0.033	0.369± 0.025	0.144± 0.034	0.198± 0.032	0.163± 0.034	0.019± 0.033
1.26–1.30	31.2± 2.0	0.067± 0.035	0.406± 0.026	0.104± 0.036	0.193± 0.034	0.079± 0.039	0.023± 0.037
1.28–1.33	29.4± 1.8	0.115± 0.032	0.403± 0.023	0.137± 0.033	0.214± 0.031	0.073± 0.033	0.076± 0.033
1.30–1.35	22.7± 1.7	0.156± 0.037	0.400± 0.027	0.172± 0.037	0.217± 0.035	0.111± 0.038	0.043± 0.038
1.33–1.37	17.2± 1.8	0.169± 0.047	0.385± 0.035	0.189± 0.049	0.186± 0.046	0.132± 0.049	0.002± 0.050
1.35–1.40	16.4± 1.6	0.198± 0.048	0.389± 0.034	0.191± 0.052	0.257± 0.049	0.108± 0.053	0.122± 0.053

poles are really needed we fitted the restricted region 935–1040 MeV with three parameters for the s wave (keeping all other waves fixed) and the region 935–1100 MeV with four parameters. Choosing different parameters each time, the striking feature was that we always found a second-sheet pole. Whether another pole was also present depended on the fit; there could be an additional nearby pole on either the third or fourth sheet. The parameters for some of these fits are given in Table XV. For all these fits the higher moments ($L \geq 4$) have a 30% absorption correction. If this correction is not made, χ^2 tend to be worse but the pole structure is not affected. We believe that our data require a second-sheet pole, but are clearly not sufficiently sensitive to be able to tell whether nearby "shadow" poles are also present. A more conclusive answer to this question will have to await higher-statistics data on the $K\bar{K}$ channel. The fact that we have much more information in the $\pi\pi$ channel may bias our results somewhat; since the additional poles observed couple weakly to the $\pi\pi$ channel, establishing their existence (or nonexistence) requires better $K\bar{K}$ data.

APPENDIX B

To facilitate any quantitative fits to our extrapolated data we include here tables of our cross sections and $\langle Y_L^0 \rangle$ up to $L = 6$ between threshold and 1.4 GeV (Tables XVI and XVII). We also include tables for $|t'| < 0.1$ GeV^2 (Table XVIII).

TABLE XVIII. Mass plot and moments ($L = 1-6$) for $|t'| < 0.1$ (GeV/c)^2.

Mass bin (GeV)	$N_{\pi\pi}$ [a]	$\langle Y_1^0 \rangle$	$\langle Y_2^0 \rangle$	$\langle Y_3^0 \rangle$	$\langle Y_4^0 \rangle$	$\langle Y_5^0 \rangle$	$\langle Y_6^0 \rangle$
0.28–0.49	24.8 ± 4.9	0.038 ± 0.011	0.022 ± 0.011	−0.003 ± 0.011	−0.001 ± 0.011	0.002 ± 0.010	0.006 ± 0.011
0.45–0.55	49.8 ± 7.0	0.099 ± 0.011	0.049 ± 0.011	−0.003 ± 0.011	−0.014 ± 0.011	−0.008 ± 0.011	0.003 ± 0.011
0.50–0.60	73.8 ± 8.0	0.110 ± 0.010	0.082 ± 0.009	−0.007 ± 0.010	−0.018 ± 0.010	−0.008 ± 0.010	0.001 ± 0.010
0.60–0.65	92.2 ± 9.6	0.133 ± 0.010	0.128 ± 0.009	0.001 ± 0.010	−0.007 ± 0.010	−0.004 ± 0.010	−0.023 ± 0.010
0.65–0.68	150.6 ± 12.2	0.139 ± 0.010	0.147 ± 0.009	0.009 ± 0.010	−0.014 ± 0.010	0.003 ± 0.010	−0.004 ± 0.010
0.68–0.70	183.5 ± 13.5	0.142 ± 0.012	0.160 ± 0.011	−0.002 ± 0.013	0.024 ± 0.012	0.012 ± 0.012	0.012 ± 0.012
0.70–0.72	275.6 ± 16.6	0.153 ± 0.010	0.159 ± 0.009	0.013 ± 0.010	−0.008 ± 0.010	0.003 ± 0.010	−0.007 ± 0.010
0.72–0.74	318.0 ± 17.8	0.143 ± 0.009	0.170 ± 0.008	−0.002 ± 0.009	−0.006 ± 0.009	0.006 ± 0.009	−0.002 ± 0.009
0.74–0.75	458.5 ± 21.4	0.158 ± 0.011	0.181 ± 0.010	0.001 ± 0.012	0.002 ± 0.012	0.016 ± 0.012	0.001 ± 0.012
0.75–0.76	573.0 ± 23.9	0.125 ± 0.011	0.168 ± 0.010	−0.010 ± 0.011	−0.011 ± 0.011	−0.025 ± 0.011	−0.014 ± 0.011
0.76–0.77	709.0 ± 26.6	0.123 ± 0.011	0.164 ± 0.010	−0.007 ± 0.012	−0.002 ± 0.012	0.003 ± 0.012	0.011 ± 0.011
0.77–0.78	712.0 ± 26.6	0.150 ± 0.012	0.201 ± 0.011	0.014 ± 0.013	0.026 ± 0.013	−0.004 ± 0.013	0.012 ± 0.013
0.78–0.79	730.0 ± 27.0	0.154 ± 0.012	0.200 ± 0.010	0.014 ± 0.012	0.010 ± 0.012	−0.010 ± 0.012	0.002 ± 0.012
0.79–0.80	633.0 ± 25.1	0.149 ± 0.012	0.200 ± 0.010	0.012 ± 0.012	0.030 ± 0.012	−0.001 ± 0.012	0.008 ± 0.012
0.80–0.82	705.0 ± 26.5	0.141 ± 0.009	0.185 ± 0.008	−0.002 ± 0.009	−0.003 ± 0.009	−0.010 ± 0.009	0.010 ± 0.009
0.82–0.84	705.0 ± 26.5	0.141 ± 0.010	0.177 ± 0.008	0.008 ± 0.010	−0.003 ± 0.010	0.010 ± 0.009	−0.007 ± 0.009
0.84–0.86	581.5 ± 24.1	0.143 ± 0.011	0.171 ± 0.009	0.020 ± 0.011	−0.001 ± 0.011	0.004 ± 0.011	−0.009 ± 0.011
0.86–0.88	487.5 ± 22.0	0.133 ± 0.012	0.180 ± 0.011	0.014 ± 0.013	0.010 ± 0.013	0.009 ± 0.013	−0.004 ± 0.013
0.88–0.90	393.5 ± 19.8	0.135 ± 0.012	0.160 ± 0.012	−0.009 ± 0.013	0.026 ± 0.013	0.017 ± 0.013	0.028 ± 0.013
0.90–0.92	306.5 ± 17.5	0.147 ± 0.014	0.170 ± 0.012	0.003 ± 0.014	0.014 ± 0.014	0.006 ± 0.014	−0.010 ± 0.014
0.92–0.95	241.5 ± 15.5	0.147 ± 0.011	0.149 ± 0.011	−0.015 ± 0.012	0.033 ± 0.012	0.005 ± 0.012	0.020 ± 0.012
0.95–0.98	218.7 ± 14.7	0.146 ± 0.013	0.163 ± 0.013	−0.021 ± 0.014	0.053 ± 0.014	0.018 ± 0.014	0.006 ± 0.014
0.98–1.02	158.5 ± 12.5	0.013 ± 0.018	0.239 ± 0.013	−0.035 ± 0.018	0.060 ± 0.018	0.021 ± 0.018	0.038 ± 0.017
1.02–1.06	101.2 ± 10.0	−0.010 ± 0.017	0.216 ± 0.014	−0.029 ± 0.017	0.059 ± 0.017	0.036 ± 0.017	0.009 ± 0.017
1.06–1.09	104.2 ± 10.2	−0.007 ± 0.019	0.238 ± 0.015	−0.038 ± 0.018	0.078 ± 0.018	0.022 ± 0.018	0.014 ± 0.018
1.09–1.12	120.6 ± 10.9	−0.002 ± 0.020	0.258 ± 0.016	−0.014 ± 0.021	0.136 ± 0.020	0.051 ± 0.021	0.046 ± 0.021
1.12–1.15	110.0 ± 10.4	−0.019 ± 0.019	0.241 ± 0.015	−0.036 ± 0.019	0.115 ± 0.017	0.044 ± 0.017	0.018 ± 0.018
1.12–1.17	124.0 ± 11.1	0.012 ± 0.013	0.240 ± 0.010	−0.014 ± 0.013	0.091 ± 0.012	0.051 ± 0.012	0.004 ± 0.013
1.15–1.20	130.0 ± 11.4	0.040 ± 0.014	0.258 ± 0.010	0.005 ± 0.014	0.099 ± 0.013	0.039 ± 0.013	0.015 ± 0.013
1.18–1.22	156.0 ± 12.4	0.064 ± 0.015	0.283 ± 0.011	0.013 ± 0.015	0.137 ± 0.014	0.026 ± 0.015	0.024 ± 0.015
1.20–1.24	165.5 ± 12.8	0.060 ± 0.014	0.265 ± 0.010	0.016 ± 0.013	0.103 ± 0.013	0.024 ± 0.013	−0.033 ± 0.013
1.22–1.26	177.5 ± 13.3	0.062 ± 0.014	0.296 ± 0.010	0.054 ± 0.013	0.134 ± 0.012	0.050 ± 0.013	−0.020 ± 0.013
1.24–1.28	205.5 ± 14.3	0.089 ± 0.013	0.314 ± 0.009	0.086 ± 0.013	0.168 ± 0.012	0.066 ± 0.013	0.013 ± 0.013
1.26–1.30	202.0 ± 14.2	0.105 ± 0.013	0.335 ± 0.009	0.090 ± 0.014	0.166 ± 0.013	0.035 ± 0.014	0.012 ± 0.014
1.28–1.33	188.5 ± 13.7	0.119 ± 0.013	0.339 ± 0.008	0.105 ± 0.013	0.167 ± 0.012	0.046 ± 0.013	0.013 ± 0.013
1.30–1.35	165.3 ± 12.8	0.136 ± 0.014	0.331 ± 0.009	0.118 ± 0.014	0.166 ± 0.013	0.045 ± 0.014	0.013 ± 0.014
1.33–1.37	116.5 ± 10.7	0.147 ± 0.017	0.322 ± 0.012	0.115 ± 0.017	0.155 ± 0.016	0.034 ± 0.018	0.005 ± 0.018
1.35–1.40	117.0 ± 10.8	0.167 ± 0.016	0.343 ± 0.011	0.133 ± 0.017	0.182 ± 0.016	0.066 ± 0.018	0.060 ± 0.018

[a] When bins are larger than 10 MeV the number given is the average number of events per 10 MeV.

†Work supported by the U. S. Atomic Energy Commission.

*Present address: Brookhaven National Laboratory, Upton, N. Y. 11973.

‡Present address: Division of Natural Sciences, University of California, Santa Cruz, Calif. 95060.

§Present address: Stanford Linear Accelerator Center, Stanford, Calif. 94305.

‖Present address: Physics Department, University of Massachusetts, Amherst, Mass. 01002.

[1]For a complete review of $\pi\pi$ scattering see: Particle Data Group, Phys. Letters 39B, 1 (1972); D. Morgan and J. Pišút, in *Low Energy Hadron Interactions*, Springer Tracts in Modern Physics, edited by G. Höhler (Springer, Berlin, 1968), Vol. 55, p. 1; J. L. Peterson, Phys. Reports 2C, 157 (1971).

[2]M. Alston-Garnjost *et al.*, Phys. Letters 36B, 152 (1970). A phenomena which could be interpreted as a rapid variation in the s wave (although at somewhat different mass ~ 940 MeV) was observed in the reaction $pp \to \pi^+\pi^-\omega$ by R. Bizzarri *et al.*, Nucl. Phys. B14, 169 (1969).

[3]S. M. Flatté *et al.*, Phys. Letters 38B, 232 (1972).

[4]C. T. Dardel *et al.*, Phys. Rev. Letters 7, 127 (1961).

[5]K. J. Foley *et al.*, Phys. Rev. Letters 11, 425 (1963).

[6]S. Protopopescu, M. Alston-Garnjost, and M. Bogdanski, Lawrence Berkeley Laboratory Group A Physics Memo 750 (unpublished).

[7]S. Protopopescu, Lawrence Berkeley Laboratory Group A Physics Memo 751 (unpublished).

[8]M. Alston-Garnjost *et al.*, Phys. Letters 33B, 607 (1970).

[9]The function $F(m, t)$ is calculated by taking the experimental cross section averaged over a bin in (t, m, M) and dividing by σ_{OPE}.

[10]H. P. Dürr and H. Pilkuhn, Nuovo Cimento 40A, 899 (1965).

[11]G. Wolf, Phys. Rev. Letters 19, 925 (1967).

[12]E. Colton, P. Schlein, and E. Gellert, Phys. Rev. D 3, 1063 (1971); T. G. Trippe, Ph.D. thesis, UCLA Report No. UCLA-1026, 1968 (unpublished).

[13]A. A. Carter *et al.*, Nucl. Phys. B26, 445 (1971).

[14]J. P. Baton, G. Laurens, and J. Reignier, Phys. Letters 33B, 528 (1970).

[15]Even with an energy-dependent analysis, one cannot determine all 12; data from other charged states are needed to separate $I=2$ and $I=0$ components.

[16]To compute $g_{\rho\omega\pi}{}^2$ we used the $\rho\omega\pi$ coupling constant calculated by M. Gell-Mann, P. Sharp, and W. G. Wagner, Phys. Rev. Letters 8, 261 (1962); the fits are rather insensitive to the value of $g_{\rho\omega\pi}{}^2$.

[17]The $I=0$ d wave cannot couple to $\omega\pi$ channels; nevertheless we allowed the background to become inelastic around 900 MeV. Results change very little if we do not allow it to become inelastic before 980 MeV.

[18]L. Roper, R. Wright, and B. Feld, Phys. Rev. 138, B190 (1965); C. J. Goebel and K. W. McVoy, *ibid.* 164, 1932 (1967).

[19]W. D. Walker *et al.*, Phys. Rev. Letters 18, 630 (1967); Baton *et al.* (Ref. 14); E. Colton *et al.*, Phys. Rev. D 3, 2028 (1971).

[20]See, for instance: Baton *et al.* (Ref. 14); Morgan and Pišút (Ref. 1).

[21]For a description of M-matrix formalism and additional references see A. Barbaro-Galtieri, in *Advances in Particle Physics*, edited by R. L. Cool and R. E. Marshak (Wiley, New York, 1968), Vol. 2, p. 212.

[22]We used the computer program OPTIME for minimizing χ^2: P. M. Eberhard and W. O. Koellner, Lawrence Radiation Laboratory Report UCRL-20159, 1970 (unpublished).

[23]E. Colton *et al.*, Phys. Rev. D 3, 2033 (1971).

[24]This statement should be qualified somewhat for the p-wave inelasticity, which can change at high masses (1100 MeV) by as much as 1 standard deviation.

[25]Although computed errors are small on the p-wave phase, there might be a systematic error introduced by the observed effect between 760 and 800 MeV (which is possibly due to ρ-ω interference). The inelasticity of the s-wave depends somewhat on the d-wave contribution to the $K\bar{K}$ channel. We do not have sufficient data to include the $K\bar{K}$ moments in a meaningful way in the analysis; however, it is clear from these moments that the s-wave must dominate below 1100 MeV (see Ref. 2).

[26]G. Laurens, Ph.D. thesis, University of Paris Report No. CEA-N-1497, 1971 (unpublished), Table XI.

[27]P. Baillon *et al.*, Phys. Letters 38B, 555 (1972). Other $\pi\pi$ phase shifts have also been reported by: B. Y. Oh *et al.*, Phys. Rev. D 1, 2494 (1970); J. T. Carroll *et al.*, Phys. Rev. Letters 28, 318 (1972); J. Gaidos *et al.*, Nucl. Phys. B46, 449 (1972); G. Grayer *et al.*, in *Experimental Meson Spectroscopy – 1972*, proceedings of the Third International Conference, Philadelphia, 1972, edited by Kwan-Wu Lai and Arthur H. Rosenfeld (A.I.P., New York, 1972). There is generally good agreement with our phase shifts up to 1.0 GeV. B. Y. Oh *et al.* and J. T. Carroll *et al.* did not have sufficient resolution to observe the rapid behavior of the s-wave phase shift (δ_0^0) near $K\bar{K}$ threshold. Above 1.0 GeV our δ_0^0 tends to be smaller than what is observed in above experiments.

[28]D. Morgan and G. Shaw, Phys. Rev. D 2, 520 (1970).

[29]B. D. Hyams *et al.*, in *Experimental Meson Spectroscopy, 1970*, edited by Charles Baltay and Arthur H. Rosenfeld (Columbia Univ. Press, New York, 1970), p. 41.

[30]W. Beusch *et al.*, in Ref. 29, p. 185.

[31]Our sample of $K^0\bar{K}^0$ events is simply too small to be able to resolve this question.

[32]F. T. Hoang, Nuovo Cimento 61A, 325 (1969).

[33]P. K. Williams, in *Experimental Meson Spectroscopy – 1972*, in Ref. 27.

[34]L. Gutay *et al.*, Nucl. Phys. B12, 31 (1969).

[35]E. P. Wigner, Phys. Rev. 98, 145 (1955).

[36]K. Gottfried and J. D. Jackson, Nuovo Cimento 34, 735 (1964).

[37]B. N. Ratcliff *et al.*, Phys. Letters 38B, 345 (1972). This article gives many references for previous results on ρ-ω interference.

[38]For the definition of the various Riemann sheets see, for example, W. R. Frazer and A. W. Hendry, Phys. Rev. 134, B1307 (1964).

[39]M. Kato and Y. Fujii, University of Tokyo report, 1972 (unpublished).

[40]The possible existence of shadow poles is discussed in R. H. Dalitz and R. G. Moorhouse, Proc. Roy. Soc. (London) A318, 279 (1970), and references therein. A general discussion of the problems in associating poles with resonances is given by G. F. Chew, in *Old and New Problems in Elementary Particles*, edited by G. Puppi (Academic, New York, 1968).